

1 **Tropical Cyclone Precipitation in the HighResMIP Atmosphere-only**
2 **Experiments of the PRIMAVERA Project**

3
4
5 Wei Zhang^{1,2*}, Gabriele Villarini¹, Enrico Scoccimarro³, Malcolm Roberts⁴, Pier Luigi Vidale⁵,
6 Benoit Vanniere⁵, Louis-Philippe Caron⁶, Dian Putrasahan⁷, Christopher Roberts⁸, Retish Senan⁸,
7 and Marie-Pierre Moine⁹

8
9
10 ¹ IIHR-Hydroscience & Engineering, The University of Iowa, Iowa City, Iowa, USA

11 ²Department of Plants, Soils and Climate, Utah State University, Utah, USA

12 ³Fondazione Centro Euro-Mediterraneo sui Cambiamenti Climatici, Bologna, Italy

13 ⁴UK Meteorological Office, Exeter, UK

14 ⁵National Centre for Atmospheric Science (NCAS), Department of Meteorology, University of
15 Reading, Reading, UK

16 ⁶Barcelona Supercomputing Center (BSC), Barcelona, Spain

17 ⁷Max Planck Gesellschaft zur Foerderung der Wissenschaften E.V. (MPI-M), Hamburg, Germany

18 ⁸European Centre for Medium-Range Weather Forecasts (ECMWF), Reading, UK

19 ⁹Climat, Environnement, Couplages, Incertitudes (CECI), Universit e de Toulouse, CNRS,
20 Cerfacs, Toulouse, France

21
22
23 Revision submitted to

24 *Climate Dynamics*

25
26 *Corresponding author:

27 Wei Zhang, Ph.D.

28 Department of Plants, Soils and Climate, Utah State University, Utah, USA.

29 Email: w.zhang@usu.edu

30 Phone: (435) 791-1101

31

32 Abstract

33 This study examines the climatology and structure of rainfall associated with tropical cyclones
34 (TCs) based on the atmosphere-only Coupled Model Intercomparison Project Phase 6 (CMIP6)
35 HighResMIP runs of the PRocess-based climate sIMulation: AdVances in high resolution
36 modelling and European climate Risk Assessment (PRIMAVERA) Project during 1979-2014.
37 We evaluate how the spatial resolution of climate models with a variety of dynamic cores and
38 parameterization schemes affects the representation of TC rainfall. These HighResMIP
39 atmosphere-only runs that prescribe historical sea surface temperatures and radiative forcings
40 can well reproduce the observed spatial pattern of TC rainfall climatology, with high-resolution
41 models generally performing better than the low-resolution ones. Overall, the HighResMIP
42 atmosphere-only runs can also reproduce the observed percentage contribution of TC rainfall to
43 total amounts, with an overall better performance by the high-resolution models. The models
44 perform better over ocean than over land in simulating climatological total TC rainfall, TC
45 rainfall proportion and TC rainfall per TC in terms of spatial correlation. All the models in the
46 HighResMIP atmosphere-only runs underestimate the observed composite TC rainfall structure
47 over both land and ocean, especially in their lower resolutions. The underestimation of rainfall
48 composites by the HighResMIP atmosphere-only runs is also supported by the radial profile of
49 TC rainfall. Overall, the increased spatial resolution generally leads to an improved model
50 performance in reproducing the observed TC rainfall properties.

51

52 **1. Introduction**

53 Tropical cyclones (TCs) are associated with extreme rainfall and are responsible for
54 extensive damages and numerous fatalities (e.g., Peduzzi et al. 2012; Rappaport 2014; Czajkowski
55 et al. 2017; Klotzbach et al. 2018; Bosma et al. 2020). For example, Hurricanes Harvey and
56 Florence serve to highlight the catastrophes that could be caused by extreme TC rainfall (e.g.,
57 Emanuel 2017; Reed et al. 2018; Risser and Wehner 2017; Van Oldenborgh et al. 2017; Wang et
58 al. 2018; Zhang et al. 2018) and are just two recent examples of a long list of catastrophic events.
59 According to the National Oceanic and Atmospheric Administration (NOAA) National Center for
60 Environmental Information (NCEI) (2020), there have been 44 TCs affecting the United States
61 causing damage in excess of one billion dollars between 1980 and 2019; in total, these events
62 caused \$945.9B (Consumer Price Index-Adjusted) and 6,502 fatalities.

63 Rainfall associated with TCs tends to be larger than for non-TC events. For instance, within
64 the novel statistical framework of the Metastatistical Extreme Value Distribution, Miniussi et al.
65 (2020) showed that the distribution of TC rainfall is different from the non-TC rainfall in the
66 Eastern United States, especially for multi-day events, and that these storms tend to result in larger
67 rainfall values. The impact of the TC rainfall is remarkable not only along the coastline, but also
68 hundreds of miles inland in terms of flooding (e.g., Villarini et al. 2014a; Khouakhi et al. 2017;
69 Aryal et al. 2018) and landslides (e.g., Bucknam et al. 2001). Despite these negative effects, they
70 can also bring water critical for groundwater recharge, water supply and drought mitigation (e.g.,
71 Abdalla and Al-Abri 2011; Kam et al. 2013; Zhang et al. 2017). It is therefore crucial that we
72 improve our understanding of the processes and characteristics of TC rainfall, which could in turn
73 lead to an improvement in its simulation and seasonal forecasting (e.g., Barlow 2011; Luitel et al.

74 2018; Liu et al. 2019; Prat and Nelson, 2016; Touma et al. 2019; Vecchi et al. 2019; Zhang et al.
75 2019).

76 There are several drivers controlling TC rainfall, including low-level vertical wind shear
77 (Corbosiero and Molinari 2003; Tang et al. 2014), terrain effects (DeHart and Houze Jr 2017;
78 Nguyen et al. 2017), TC structure (Chen et al. 2006; Hence and Houze Jr 2012; Yu et al. 2017),
79 sea surface temperature (Langousis and Veneziano 2009; Lin et al. 2015), and atmospheric
80 aerosols (Wang et al. 2014; Zhao et al. 2018). Over the years and thanks to advances in observing
81 capabilities, major progress has been made in understanding the temporal and spatial components
82 of TC rainfall through satellite monitoring (e.g., Rios Gaona et al. 2018; Jiang and Zipser 2010;
83 Jiang et al. 2011; Prat and Nelson 2013b), radar data (e.g., Villarini et al. 2011; Bao et al. 2017;
84 Janapati et al. 2020) and rain gauges (e.g., Khouakhi et al. 2017; Villarini and Denniston 2016).
85 Overall, these studies indicate that TC rainfall substantially contributes to the mean and extreme
86 precipitation events, particularly along coastal regions (Khouakhi et al. 2017; Shepherd et al. 2007;
87 Knight et al. 2009; Prat et al. 2013; Villarini et al. 2011; 2014b). In addition to observations,
88 numerical models with the capability of resolving TCs have been used to examine TC rainfall (e.g.,
89 Daloz et al. 2010; Kim et al. 2018; Liu et al. 2018; 2019; Moon et al. 2020; Scoccimarro et al.
90 2014; 2017a; Villarini et al. 2014; Zhang et al. 2019). While climate models can well simulate the
91 overall climatology of TC rainfall (e.g., Zhang et al. 2019), these models have limitations in
92 simulating individual events and exhibit strong discrepancies in the simulated pattern and
93 magnitude of TC rainfall (Scoccimarro et al. 2017c; Wright et al. 2015; Zhang et al. 2019).

94 In the climate modeling community, special attention has been paid to the examination of
95 the impacts of horizontal resolution on TC simulations (e.g., Zhao et al. 2009; Caron et al. 2011;
96 Manganello et al. 2012; Wehner et al. 2014; Roberts et al. 2015; 2020; Murakami et al. 2015;

97 Zhang et al. 2015; Vecchi et al. 2019). Despite these efforts, it is difficult to generalize the
98 conclusions of these studies because of the differences in experimental design, tracking algorithm,
99 and model parameters. While much of the focus has been on the role of resolution in terms of TC
100 characteristics, recently Zhang et al. (2019) assessed the role of horizontal resolution of two
101 climate models (i.e., the Geophysical Fluid Dynamics Laboratory (GFDL) Forecast-Oriented Low
102 Ocean Resolution version of CM2.5 (FLOR, ~50km) and the High-Resolution FLOR (HiFLOR,
103 ~25km)) in simulating TC rainfall and found that the high-resolution model (~25km) outperforms
104 the low-resolution model (~50km) in reproducing and forecasting TC rainfall.

105 Based on this overview, numerical models have advanced our understanding of TC rainfall
106 and provided insights into future projection of TC rainfall; however, there is a very limited number
107 of climate models that can properly resolve TCs. Although there are individual studies that have
108 focused on the impacts of horizontal resolution on TCs, there are many differences in the models'
109 setups and simulations that would lead to the different behaviors in simulating TC rainfall,
110 representing a critical obstacle in terms of the generalization of the results from different studies.
111 Most conclusions drawn on the projection of TC rainfall are based on the fifth phase of the Coupled
112 Model Intercomparison Project (CMIP5)'s climate models with spatial resolution of ~1-3 degrees,
113 which are too coarse to properly resolve TCs. To overcome this limitation, the sixth phase of the
114 Coupled Model Intercomparison Project (CMIP6) High Resolution Model Intercomparison
115 Project (HighResMIP) provides multi-model and multi-resolution simulations to the scientific
116 community (Haarsma et al. 2016). Using the CMIP6 HighResMIP protocol, the European Union
117 Horizon 2020's PProcess-based climate sIMulation: AdVances in high resolution modelling and
118 European climate Risk Assessment (PRIMAVERA) project has contributed global atmospheric
119 general circulation models (AGCM) simulations at a CMIP6-type resolution (i.e., ~100 km) and

120 higher (e.g., ~25 km), which allow us to examine TCs and understand the robustness of changes
121 in TC rainfall across a wide range of numerical models and spatial resolutions (Roberts et al. 2020).
122 Roberts et al. (2020) examined the roles of horizontal resolution in simulating TCs in terms of
123 frequency, intensity, structure and accumulated cyclone energy across these models. In addition,
124 Vanniere et al. (2020) focused on the sensitivity of moisture budget associated with TC rainfall to
125 different spatial resolution of the climate models in this project. This study will take advantage of
126 the simulations archived in the PRIMAVERA project to evaluate the fidelity of these climate
127 models in representing TC rainfall and the dependence of skill on resolution.

128 The remainder of the manuscript is organized as follows. Section 2 describes data and
129 methods, followed by Section 3 that presents results based on observations and models. Finally,
130 Section 4 summarizes the main points and concludes the study.

131

132 **2. Data and Methods**

133 TC observations are obtained from the International Best Track Archive for Climate
134 Stewardship (IBTrACS) version 4 with longitude, latitude, time, intensity (i.e., maximum
135 sustained wind) and central pressure at the six-hour time scale (Knapp et al. 2010). Rainfall is
136 obtained from the Multi-Source Weighted-Ensemble Precipitation, version 2 (MSWEP V2) which
137 is a gridded precipitation dataset available during 1979–2017 with high spatial (0.1°) and temporal
138 (three-hour) resolution (Beck et al. 2017a,b). TC rainfall is defined as the rainfall at 6-hour
139 intervals within a 500-km radius of a TC center by accounting for the rainfall covering the inner
140 core of the TC and the adjacent rainbands (e.g., Dare et al. 2012; Villarini et al. 2014b; Zhang et
141 al. 2019). Although there might be some uncertainties in extracting TC rainfall using this radius at
142 each 6-hour time step, the selection of this radius is also supported by the fact that most

143 precipitation associated with TCs occurs within 5° (~500km) from the center of the storm for
144 climate models (Trenberth et al. 2007; Vanniere et al. 2020). The TC-rainfall composites are the
145 composites of the extracted TC rainfall using the 500-km radius and we process the TC rainfall for
146 three scenarios: land and ocean, only land and only ocean.

147 We use the HighResMIP atmosphere-only simulations performed by the Met Office
148 Hadley Centre's HadGEM3-GC313-GC31 (Roberts et al. 2019a), the European Centre for
149 Medium-Range Weather Forecasts Integrated Forecasting System (ECMWF IFS) (Roberts et al.
150 2018), CNRM-CM6-1 developed by Centre National de Recherches Météorologiques—Groupe
151 d'études de l'Atmosphère Météorologique/Centre Européen de Recherche et de Formation
152 Avancée (Voldoire et al. 2019), the Fondazione Centro Euro-Mediterraneo sui Cambiamenti
153 Climatici Climate Model Version 2 (CMCC-CM2-(V)HR4; Cherchi et al. 2019, Scoccimarro et
154 al. 2020), the EC-EARTH3 Consortium's EC-Earth3P (Haarsma et al. 2019), and Max Planck
155 Institute Earth System Model version 1.2 (MPI-ESM1-2; Gutjahr et al. 2019) (see Table 1 for
156 details). The atmosphere-only HighResMIP experiments are forced by the historical estimates of
157 sea surface temperature, sea ice, and radiative forcings (as described in Haarsma et al. 2016). It
158 should be noted that the atmosphere-only HighResMIP simulations are slightly different from the
159 CMIP6 (Eyring et al. 2016) AMIP experiments (Gates et al. 1999) in terms of forcing of aerosol,
160 sea surface temperature and sea ice (Roberts et al. 2020). We obtain the model simulations
161 archived in the Earth System Grid Federation (ESGF) nodes, including Roberts (HadGEM3-
162 GC31; 2017a, 2017b, 2017c), Roberts et al. (ECMWF-IFS; 2017a, 2017b), Voldoire (CNRM-
163 CM6-1; 2017, 2018), Scoccimarro et al. (CMCC-CM2-(V)HR4; 2017b, 2017c), EC-Earth
164 Consortium (EC-Earth3P; 2018a, 2018b), and von Storch et al. (MPI-ESM1-2; 2017, 2019). In
165 addition, the TC tracks obtained from these datasets are available from Roberts (2019b).

166 To facilitate the comparison of the simulation of TC rainfall, the climate model outputs are
167 grouped into high-, medium- and low- spatial-resolution models (Table 1). While ECMWF IFS
168 data provided to the HighResMIP simulations are based on a reduced-resolution regular grid, the
169 original ECMWF-IFS output uses the cubic octahedral reduced Gaussian grid, with resolutions of
170 Tco399 (~25 km) and Tco199 (~50 km) for the HR and LR configurations, respectively. Therefore,
171 we include ECMWF-IFS-HR/ECMWF-IFS-LR in the high-resolution/middle-resolution group,
172 respectively (Table 1). TC tracks with latitude, longitude, time and intensity are derived by
173 applying a tracker called “TRACK” to the simulations performed by these models (Hodges et al.
174 2017). This tracker uses the 6-hourly relative vorticity at the 850-, 700-, and 600-hPa levels for
175 tracking TCs and has been widely used in TC studies (Hodges et al. 2017).

176 We evaluate the performance of these models in simulating TC rainfall across the globe,
177 and for the basins (Table 2): western North Pacific, eastern North Pacific, North Atlantic, South
178 Atlantic, North Indian Ocean, South-West Indian Ocean and South Pacific & Australia. We use
179 spatial correlation and root mean square error (RMSE) as quantitative metrics for the evaluation.
180 Because there is no named storm in South Atlantic in observations during the study period (Table
181 S1), we do not include the analysis of spatial correlation and RMSE between observations and
182 models for this basin.

183 Beyond the high resolution of these models, a major advantage of the PRIMAVERA
184 Project is the consistency of the simulations and outputs: all the models were run using the same
185 forcings, and the tracking of the storms is the same across models, allowing for a direct comparison
186 in terms of model performance and on the role of resolution.

187

188 **3. Results**

189 3.1 Total TC rainfall

190 The annual total TC rainfall averaged over 1979-2014 in the observations exhibits regional
191 differences across ocean basins (Figure 1). For example, the annual TC rainfall is the highest in
192 the western North Pacific, followed by the eastern North Pacific. The annual TC rainfall in the
193 North Atlantic is lower than in the eastern North Pacific and little TC rainfall is observed in the
194 South Atlantic (Figure 1). Qualitatively, the climate models tend to capture the overall spatial
195 climatological pattern of TC rainfall in the observations; this is particularly true in relation to the
196 areas in the North Pacific characterized by larger TC rainfall values compared to the rest of the
197 basins (Figure 2). The GCMs generally produce spurious TC rainfall in the South Atlantic (Figure
198 2). Specifically, CMCC-CM2-VHR4, EC-Earth3P-HR, ECMWF-IFS-HR, and ECMWF-IFS-LR
199 reproduce well the total TC rainfall amount across different basins (Figure 2), consistent with
200 spatial correlation and RMSE between observed and simulated total TC rainfall (Tables 3-4). In
201 addition, CNRM-CM6-1-HR, CNRM-CM6-1, HadGEM3-GC31-HM, HadGEM3-GC31-MM,
202 HadGEM3-GC31-LM point to an overestimation of the total TC rainfall, while EC-Earth3P,
203 MPIESM1-2-XR and MPIESM1-2-HR to an underestimation of the total TC rainfall across all
204 basins (Figure 2). This is consistent with the results of TC track density (Figure 3), which is also
205 documented in Roberts et al. (2020) which reported that EC-Earth3P and MPIESM1-2-XR
206 underestimate TC track density. Vanniere et al. (2020) also found that TC activity/frequency plays
207 an important role in explaining the differences in total TC rainfall between high-resolution and
208 low-resolution models. Based on the above results, high-resolution models tend to perform better
209 in reproducing the observed climatology of TC rainfall. Overall, increase in model resolution tends
210 to produce a higher amount of total TC rainfall for the CMCC models, EC-Earth3P models,
211 HadGEM3-GC31 (i.e., HadEM3-GC31-HM and HadGEM3-GC31-LM) and ECMWF-IFS

212 models, while TC rainfall shows little to no sensitivity to spatial resolution in CNRM-CM6-1 and
213 MPIESM1-2 models (Figure 2). Four of the six models exhibit remarkable differences in TC
214 rainfall between high-resolution and low-resolution models while the other two show similar
215 results (Figure 2). The low sensitivity to spatial resolution in CNRM-CM6-1 and MPIESM1-2
216 models may be due to low absolute resolution in the models, the high-resolution version of which
217 is around ~50km (Table 1).

218 **3.2 Contribution of TC rainfall to Total Rainfall**

219 In addition to total TC rainfall, we also examine the percentage contribution of TC rainfall
220 to total rainfall. In the observations, the percentage contribution presents remarkable regional
221 differences with the highest values in the western and eastern North Pacific (Figure 4), consistent
222 with total TC rainfall (Figure 1). Climate models exhibit strong discrepancies in the capability of
223 reproducing the observed percentage contribution (Figure 4). Globally, EC-Earth3P-HR,
224 ECMWF-IFS-HR, ECMWF-IFS-LR, HadGEM3-GC31-HM, HadGEM3-GC31-MM, and
225 HadGEM3-GC31-LM reproduce well the observed contribution of TC rainfall in terms of RMSE.
226 CMCC-CM2-VHR4, EC-Earth3P-HR, EC-Earth3P, ECMWF-IFS-HR, ECMWF-IFS-LR, and
227 HadGEM3-GC31 models produce spatial correlations greater than 0.8, suggesting a good
228 performance (Table 5). The models exhibit marked regional differences. For example, CNRM-
229 CM6-1-HR and CNRM-CM6-1 reproduce well the observed contribution of TC rainfall in the
230 western North Pacific, and the performance of these models is not very promising in the North
231 Indian Ocean (Figure 4 and Tables 5-6). High-resolution models generate a higher contribution,
232 more similar to the observations except for MPIESM1-2-XR/MPIESM1-2-HR and CNRM-CM6-
233 1-HR/CNRM-CM6-1, which produce similar percentage contributions between high-resolution
234 and low-resolution models (Figure 4). Therefore, most of the high-resolution models perform

235 better than their low-resolution counterparts in reproducing the global fractional contribution
236 (Figure 4 and Table 5). To further understand the proportion of TC rainfall, we also examine the
237 bias in the models (Figure 5). Overall, the bias in TCR proportion (Figure 5) is mainly due to the
238 bias in TC rainfall (Figure 2), rather than total precipitation (Figure 6).

239 **3.3 TC rainfall per track density**

240 All the models in the PRIMAVERA Project underestimate the amount of TC rainfall per
241 track density (i.e., total TC rainfall divided by track density) in the observations (Figure 7).
242 Therefore, given that the TC rainfall amounts identified in the models were similar to the
243 observations, it means that there are generally more storms in the models than in the observational
244 records. As we compare the results between the different resolutions of the models, some models
245 (i.e., CMCC-CM2, CNRM and HadGEM3-GC31) have a tendency for lower-resolution versions
246 to have larger per-TC rainfall amounts. This counter-intuitive results may be due to the fact that
247 lower TC density is produced by low-resolution simulations than in the high-resolution ones
248 (Figure 3), consistent with Vanniere et al. (2020) showing that rainfall per TC is biased high in
249 low-resolution models. The spatial correlation between observed and simulated amount of TC
250 rainfall per track density (Table S2) is lower than for total TC rainfall or fractional contribution,
251 with most of the correlation coefficients that are not statistically significant. Among the models
252 used in this study, the CNRM models perform the best in simulating the rainfall per track density
253 (Figure 7 and Tables S2-3) and this is consistent with the fact that CNRM performs well in
254 simulating the strongest TCs (Roberts et al. 2020).

255 **3.4 TC rainfall over Ocean and Land**

256 We also evaluate the performance of the models in simulating climatological TC rainfall
257 over ocean and land. Overall, the models perform better in simulating total TC rainfall, TC rainfall

258 proportion and TC rainfall per TC over ocean than over land in terms of spatial correlation (Tables
259 S4-6). However, the models generate a larger RMSE for the three metrics over ocean than over
260 land (Tables S4-6), and this may be due to a large climatology of TC rainfall over ocean (Figure
261 1).

262 **3.5 Composites and Profile of TC rainfall**

263 We process the composite TC rainfall (within the 500-km radius of TC center) at 6-hour
264 time step for all the storms, those in the northern hemisphere and those in the southern hemisphere
265 in observations and climate models (Figure 8). The composite TC rainfall (within the 500-km
266 radius) at 6-hourly intervals in the observations is higher than model simulations over ocean and
267 land (Figure 8). CMCC-CM2-VHR4 performs the best in reproducing the composite TC rainfall
268 over ocean and land, with larger precipitation values closer to the center of circulation of the
269 storms, even though the size of the TCs tends to be smaller than in the observations and in other
270 models (e.g., CNRM). There is also a tendency for the storms in the northern hemisphere to exhibit
271 larger rainfall values compared to those in the southern hemisphere, consistent with the
272 observations. The high-resolution models produce larger composite TC rainfall rate than low-
273 resolution models, which tend to spread rainfall over larger distances from the center of circulation
274 of the TCs (Figure 8). In addition, we compare the composite rainfall in the 200 strongest storms
275 in observations and the low- and high-resolution models. Overall, the composite rainfall rate in the
276 high-resolution models is larger than in the low-resolution ones except for the MPI-ESM 1-2
277 models that simulate similar composite TC rainfall (Figure 9). The differences in composite TC
278 rainfall of the 200 strongest TCs between low-resolution and high-resolution models (Figure 9)
279 are more remarkable than the results for all TCs (Figure 8), and this may be due to a large portion
280 of intense TCs in the high-resolution models than low-resolution ones (Roberts et al. 2020). To

281 assess whether the models' skill is different in simulating TC rainfall over ocean or land mass, we
282 examine the composite TC rainfall over ocean and land, separately. The composite TC rainfall
283 over the ocean exhibits similar characteristics as those over land & ocean, with a well-defined
284 center of circulation, albeit presenting a slightly higher magnitude (Figure 10). While almost all
285 the models underestimate the composite TC rainfall over land compared with observations (Figure
286 11), CMCC-CM2-VHR4 slightly overestimates the center of composite TC rainfall over land and
287 HadGEM3-GC31-HM produces a similar magnitude of composite TC rainfall over land (Figure
288 11). Given the fact that TCs in models have a shorter path on land than the observations (due to
289 the tracker) and TC rainfall rate over ocean is larger than over land, this suggests that the
290 underestimation of composite TC rainfall in models might be even more pronounced than the
291 results here. Based on these results, there are no large differences in the performance of the models
292 in reproducing composite TC rainfall over ocean or land. Note that the composite rainfall patterns
293 are consistent with the results in Kim et al. (2018) which examined the composite TC rainfall
294 across a family of Geophysical Fluid Dynamics Laboratory (GFDL) models.

295 In addition to the examination of the composite TC rainfall, we compute the radial profile
296 of TC rainfall across different models grouped by spatial resolution (Table 1) and land/ocean
297 masks (Figure 12). Consistent with the results in Figures 8-11, the observed rainfall tends to be
298 higher than what is generated by these models, especially closer to their center of circulation; this
299 statement is valid regardless of resolution, and whether over land or ocean. The observed TC
300 rainfall over the oceans tends to peak within 100 km from the center of the storm, and then to
301 rapidly decrease as we move further away. This feature is generally well captured by the models,
302 with the CMCC-CM2-VHR4 tending to perform the best among high-resolution groups. Among
303 the mid-resolution group, HadGEM3-GC31-MM exhibits the highest skill in simulating the radial

304 profile of TC rainfall, while CNRM-CM6-1 tends to perform the best among the low-resolution
305 group (Figure 12). The model performance in terms of TC rainfall when the storms are over land
306 is similar to that mentioned for the storms over the ocean, even though the rainfall amounts tend
307 to be smaller and to decrease more slowly as they progress inland. The radial profile of TC rainfall
308 is consistent with Kim et al. (2018) and Moon et al. (2020) in terms of pattern and magnitude of
309 TC rainfall across different climate models.

310

311 **4. Conclusion**

312 TC rainfall has been a challenge for climate modeling community because this metric is
313 associated with TC genesis, track, and intensity. By taking advantage of the European Union
314 Horizon 2020's PRIMAVERA Project, we have examined the skill of state-of-the-art global
315 climate models in reproducing several aspects of the rainfall associated with these storms in
316 HighResMIP atmosphere-only experiments and assessed the dependence of the skill on model
317 resolution.

318 In general, high-resolution models perform better than their lower resolution counterparts
319 in reproducing several characteristics of the TC distribution. They tend to provide a more realistic
320 representation of the observations both in terms of patterns and amounts, except for average TC
321 rainfall per track density for which low-resolution models seem better for some models. The
322 simulation of TC rainfall by these models exhibits remarkable regional differences and
323 discrepancies. For example, the CMCC-CM2 and ECMWF-IFS models reproduce the total TC
324 rainfall found in observations, while they slightly underestimate their percentage contribution and
325 overall amount per track density. By contrast, CNRM-CM6-1 and HadGEM3-GC31 models
326 overestimate total TC rainfall, but they reproduce the fractional contribution of TC rainfall to total

327 rainfall. MPIESM1-2 and EC-Earth3P models underestimate most of the metrics associated with
328 TC rainfall. Overall, the models perform better in simulating climatological total TC rainfall, TC
329 rainfall proportion and TC rainfall per TC over ocean than over land in terms of spatial correlation.
330 However, the models generate larger RMSE for the three metrics over ocean than over land,
331 probably due to a larger climatology of TC rainfall over ocean.

332 When we stratified the results of composite TC rainfall across land and ocean, we did not
333 find any large changes in performance of these models, as they were able to reproduce the overall
334 patterns albeit with lower rainfall magnitudes. Overall, CMCC-CM2-VHR4 performs the best in
335 simulating the radial profile of TC rainfall among the high-resolution model group, while
336 HadGEM3-GC31-MM (CNRM-CM6-1) exhibits the highest skill in simulating the radial profile
337 of TC rainfall in the mid-resolution (low-resolution) group.

338 While most models tend to improve their performance as we increase their horizontal
339 resolution, the CNRM-CM6-1 and MPIESM1-2 models are two exceptions, producing similar
340 results in their low- and high- resolution versions. Such similar performances between high-
341 resolution and low-resolution climate models need to be further investigated from the perspective
342 of convection, circulation and TC dynamics. For example, Vanniere et al (2020) investigated
343 possible mechanisms by examining moisture budget, and found that the distribution of
344 precipitation per TC averaged in a 5-degree radial cap does not change significantly, which can be
345 explained by the large-scale balance that shapes the moisture budget of TCs.

346 In summary, our findings indicate that the investment in performing the high-resolution
347 simulations with these models has been paid off in terms of the gained realism in reproducing TC
348 rainfall. As we increase the horizontal resolution and we improve the description of the processes

349 at play, we expect to further improve the simulation of these storms, providing basic information
350 towards our preparation, mitigation and response efforts.

351
352

353 **Acknowledgements:**

354

355 We thank the two anonymous reviewers for insightful comments. Wei Zhang and Gabriele

356 Villarini acknowledge support by the National Science Foundation under Grant EAR-1840742.

357 MR, LPC, CDR, RS, PLV, ES, BV, DP, and MPM acknowledge funding from the PRIMAVERA

358 project, funded by the European Union's Horizon 2020 programme under Grant Agreement no.

359 641727.

360

361 **Reference:**

- 362
- 363 Abdalla, O., and R. bin Y. Al-Abri, (2011). Groundwater recharge in arid areas induced by
364 tropical cyclones: lessons learned from Gonu 2007 in Sultanate of Oman. *Environ Earth Sci*,
365 63, 229–239. <https://doi.org/10.1007/s12665-010-0688-y>
- 366 Aryal, Y.N., G. Villarini, W. Zhang, and G.A. Vecchi, Long term changes in flooding and heavy
367 rainfall associated with North Atlantic tropical cyclones: Roles of the North Atlantic
368 Oscillation and El Niño-Southern Oscillation, *Journal of Hydrology*, 559, 698-710, 2018.
- 369 Bao, X., D. Wu, X. Lei, L. Ma, D. Wang, K. Zhao, and B. J.-D. Jou, 2017: Improving the
370 extreme rainfall forecast of Typhoon Morakot (2009) by assimilating radar data from Taiwan
371 Island and mainland China. *Journal of Meteorological Research*, **31**, 747-766.
- 372 Barlow, M., 2011: Influence of hurricane-related activity on North American extreme
373 precipitation. *Geophysical Research Letters*, 38 , L04705.
- 374 Beck, H. E., A. I. Van Dijk, V. Levizzani, J. Schellekens, D. Gonzalez Miralles, B. Martens, and
375 A. De Roo, 2017a: MSWEP: 3-hourly 0.25 global gridded precipitation (1979-2015) by
376 merging gauge, satellite, and reanalysis data. *Hydrology and Earth System Sciences*, **21**, 589-
377 615.
- 378 Bosma, C. D., D. B. Wright, P. Nguyen, J. P. Kossin, D. C. Herndon, and J. M. Shepherd, 2020:
379 An intuitive metric to quantify and communicate tropical cyclone rainfall hazard. *Bulletin of*
380 *the American Meteorological Society*, 101, E206-E220.
- 381 Beck, H. E., and Coauthors, 2017b: Global-scale evaluation of 22 precipitation datasets using
382 gauge observations and hydrological modeling. *Hydrology and Earth System Sciences*, **21**,
383 6201.
- 384 Bucknam, R. C., J.A. Coe, M.M. Chavarria, J.W. Godt, A.C. Tarr, ... , and M.L. Johnson (2001).
385 Landslides triggered by Hurricane Mitch in Guatemala - Inventory and discussion. USGS
386 Report Number 2001-443.
- 387 Caron, L-P, CG Jones and K Winger (2011) Impact of resolution and downscaling technique in
388 simulating recent Atlantic tropical cyclone activity. *Climate Dynamics*, 5, 869-892. doi:
389 10.1007/s00382-010-0846-7.
- 390 Chavas, D. R., N. Lin, W. Dong, and Y. Lin (2016), Observed Tropical Cyclone Size Revisited,
391 *Journal of Climate*, 29(8), 2923-2939, doi:10.1175/jcli-d-15-0731.1.
- 392 Chen, S. S., J. A. Knaff, and F. D. Marks Jr, 2006: Effects of vertical wind shear and storm
393 motion on tropical cyclone rainfall asymmetries deduced from TRMM. *Monthly Weather*
394 *Review*, **134**, 3190-3208.
- 395 Cherchi, A., and Coauthors, 2019: Global Mean Climate and Main Patterns of Variability in the
396 CMCC-CM2 Coupled Model. *Journal of Advances in Modeling Earth Systems*, **11**, 185-209.
- 397 Corbosiero, K. L., and J. Molinari, 2003: The relationship between storm motion, vertical wind
398 shear, and convective asymmetries in tropical cyclones. *Journal of the Atmospheric Sciences*,
399 **60**, 366-376.
- 400 Czajkowski, J., G. Villarini, M. Montgomery, E. Michel-Kerjan, and R. Goska, Assessing
401 current and future freshwater flood risk from North Atlantic tropical cyclones via insurance
402 claims, *Scientific Reports*, 7, 1-10, 2017.
- 403 Daloz, A. S., F. Chauvin, and F. Roux, 2010: Tropical cyclone rainfall in the observations,
404 reanalysis and ARPEGE simulations in the North Atlantic Basin. *Hurricanes and climate*
405 *change*, Springer, 57-79.

406 Dare, R. A., N. E. Davidson, and J. L. McBride, 2012: Tropical cyclone contribution to rainfall
407 over Australia. *Monthly Weather Review*, **140**, 3606-3619.

408 DeHart, J. C., and R. A. Houze Jr, 2017: Orographic modification of precipitation processes in
409 Hurricane Karl (2010). *Monthly Weather Review*, **145**, 4171-4186.

410 EC-Earth Consortium (EC-Earth), 2018a: EC-Earth-858 Consortium EC-Earth3P model output
411 prepared for CMIP6 HighResMIP. Earth System Grid Federation. <http://cera860>
412 www.dkrz.de/WDCC/meta/CMIP6/CMIP6.HighResMIP.EC-Earth-Consortium.EC861Earth3P

413 EC-Earth Consortium (EC-Earth), 2018b: EC-Earth-Consortium EC-Earth3P-HR model output
414 prepared for CMIP6 HighResMIP. Earth System Grid Federation. <http://cera->
415 [www.dkrz.de/WDCC/meta/CMIP6/CMIP6.HighResMIP.EC-Earth-Consortium.EC-Earth3P-](http://www.dkrz.de/WDCC/meta/CMIP6/CMIP6.HighResMIP.EC-Earth-Consortium.EC-Earth3P-HR)
416 [HR](http://cera-)

417 Emanuel, K., 2017: Assessing the present and future probability of Hurricane Harvey's rainfall.
418 *Proceedings of the National Academy of Sciences*, **114**, 12681-12684.

419 Gates, W. L., and Coauthors, 1999: An overview of the results of the Atmospheric Model
420 Intercomparison Project (AMIP I). *Bulletin of the American Meteorological Society*, **80**, 29-
421 56.

422 Gutjahr, O., and Coauthors, 2019: Max Planck Institute Earth System Model (MPI-ESM1.2) for
423 the High-Resolution Model Intercomparison Project (HighResMIP). *Geosci. Model Dev.*, **12**,
424 3241-3281.

425 Haarsma, R. J., and Coauthors, 2016: High Resolution Model Intercomparison Project
426 (HighResMIP v1.0) for CMIP6. *Geosci. Model Dev.*, **9**, 4185-4208.

427 Hence, D. A., and R. A. Houze Jr, 2012: Vertical structure of tropical cyclone rainbands as seen
428 by the TRMM Precipitation Radar. *Journal of the atmospheric sciences*, **69**, 2644-2661.

429 Hodges, K., A. Cobb, and P. L. Vidale, 2017: How well are tropical cyclones represented in
430 reanalysis datasets? *Journal of Climate*, **30**, 5243-5264.

431 Janapati, J., and Coauthors, 2020: Raindrop Size Distribution Characteristics of Indian and
432 Pacific Ocean Tropical Cyclones Observed at India and Taiwan Sites. *Journal of the*
433 *Meteorological Society of Japan. Ser. II.*

434 Jiang, H., and E. J. Zipser, 2010: Contribution of tropical cyclones to the global precipitation
435 from eight seasons of TRMM data: Regional, seasonal, and interannual variations. *Journal of*
436 *climate*, **23**, 1526-1543.

437 Jiang, H., C. Liu, and E. J. Zipser, 2011: A TRMM-based tropical cyclone cloud and
438 precipitation feature database. *Journal of applied meteorology and climatology*, **50**, 1255-
439 1274.

440 Kam, J., J. Sheffield, X. Yuan, and E. F. Wood, 2013: The Influence of Atlantic Tropical
441 Cyclones on Drought over the Eastern US (1980-2007), *J. Climate*, 26 (10), 3067-3086.

442 Kim, D., and Coauthors, 2018: Process-oriented diagnosis of tropical cyclones in high-resolution
443 GCMs. *Journal of Climate*, 31, 1685-1702.

444 Khouakhi, A., G. Villarini, and G. A. Vecchi, 2017: Contribution of tropical cyclones to rainfall
445 at the global scale. *Journal of Climate*, **30**, 359-372.

446 Klotzbach, P.J., S.G. Bowen, R. Pielke Jr., and M. Bell, Continental U.S. hurricane landfall
447 frequency and associated damage: Observations and future risks, *Bulletin of the American*
448 *Meteorological Society*, 99(7), 1359-1376, 2018.

449 Knapp, K. R., M. C. Kruk, D. H. Levinson, H. J. Diamond, and C. J. Neumann, 2010: The
450 International Best Track Archive for Climate Stewardship (IBTrACS). *Bulletin of the*
451 *American Meteorological Society*, **91**, 363-376.

452 Knight, D. B., and R. E. Davis, 2009: Contribution of tropical cyclones to extreme rainfall events
453 in the southeastern United States. *Journal of Geophysical Research: Atmospheres*, **114**.

454 Lin, Y., M. Zhao, and M. Zhang, 2015: Tropical cyclone rainfall area controlled by relative sea
455 surface temperature. *Nature communications*, **6**, 1-7.

456 Liu, M., G. A. Vecchi, J. A. Smith, and H. Murakami, 2018: Projection of landfalling–tropical
457 cyclone rainfall in the Eastern United States under anthropogenic warming. *Journal of*
458 *Climate*, **31**, 7269-7286.

459 Liu, M., G. A. Vecchi, J. A. Smith, and T. R. Knutson, 2019: Causes of large projected increases
460 in hurricane precipitation rates with global warming. *npj Climate and Atmospheric Science*,
461 **2**, 38.

462 Luitel, B., G. Villarini, and G.A. Vecchi, Verification of the skill of numerical weather
463 prediction models in forecasting rainfall from U.S. landfalling tropical cyclones, *Journal of*
464 *Hydrology*, 556, 1026-1037, 2018.

465 Manganello, J. V., and Coauthors, 2012: Tropical cyclone climatology in a 10-km global
466 atmospheric GCM: toward weather-resolving climate modeling. *Journal of Climate*, **25**,
467 3867-3893.

468 Miniussi, A., G. Villarini, and M. Marani, Analyses through the metastatistical extreme value
469 distribution identify contributions of tropical cyclones to rainfall extremes in the eastern US,
470 *Geophysical Research Letters*, 47(7), e2020GL087238, 1-9, 2020.

471 Moon, Y., and Coauthors, 2020: Azimuthally averaged wind and thermodynamic structures of
472 tropical cyclones in global climate models and their sensitivity to horizontal resolution.
473 *Journal of Climate*, **33**, 1575-1595.

474 Murakami, H., and Coauthors, 2015: Simulation and prediction of category 4 and 5 hurricanes in
475 the high-resolution GFDL HiFLOR coupled climate model. *Journal of Climate*, **28**, 9058-
476 9079.

477 Nguyen, L. T., R. F. Rogers, and P. D. Reasor, 2017: Thermodynamic and kinematic influences
478 on precipitation symmetry in sheared tropical cyclones: Bertha and Cristobal (2014). *Monthly*
479 *Weather Review*, **145**, 4423-4446.

480 NOAA National Centers for Environmental Information (NCEI) U.S. Billion-Dollar Weather
481 and Climate Disasters (2020). <https://www.ncdc.noaa.gov/billions/>, DOI: 10.25921/stkw-
482 7w73

483 Peduzzi, P., B. Chatenoux, H. Dao, A. De Bono, C. Herold, J. Kossin, F. Mouton, and O.
484 Nordbeck, Global trends in tropical cyclone risk, *Nature Climate Change*, **2**, 289-294, 2012.

485 Prat, O. P., and B. R. Nelson, 2013a: Precipitation contribution of tropical cyclones in the
486 southeastern United States from 1998 to 2009 using TRMM satellite data. *Journal of*
487 *Climate*, **26**, 1047-1062.

488 —, 2013b: Mapping the world's tropical cyclone rainfall contribution over land using the
489 TRMM Multi-satellite Precipitation Analysis. *Water Resources Research*, **49**, 7236-7254.

490 —, 2016: On the link between tropical cyclones and daily rainfall extremes derived from
491 global satellite observations. *Journal of Climate*, **29**, 6127-6135.

492 Rappaport, E.N., Fatalities in the United States from Atlantic tropical cyclones, 2014: New data
493 and interpretation, *Bulletin of the American Meteorological Society*, **95(3)**, 341-346.

494 Reed, K. A., A. Standfield, M. F. Wehner, and C. M. Zarzycki, 2018: The human influence on
495 Hurricane Florence. *website accessed October*.

496 Rios Gaona, M.F., G. Villarini, W. Zhang, and G.A. Vecchi, The added value of IMERG in
497 characterizing rainfall in tropical cyclones, *Atmospheric Research*, **209**, 95-102, 2018.

498 Risser, M. D., and M. F. Wehner, 2017: Attributable human-induced changes in the likelihood
499 and magnitude of the observed extreme precipitation during Hurricane Harvey. *Geophysical*
500 *Research Letters*, **44**, 12,457-412,464.

501 Roberts, C. D., R. Senan, F. Molteni, S. Boussetta, M. Mayer, and S. P. Keeley, 2018: Climate
502 model configurations of the ECMWF-Integrated Forecasting System (ECMWF-IFS cycle
503 43r1) for HighResMIP. *Geoscientific model development*, **11**, 3681-3712.

504 Roberts, C. D., R. Senan, F. Molteni, S. Boussetta, S. Keeley, 2017a: ECMWF ECMWF-IFS-LR
505 model output prepared for CMIP6 HighResMIP. Version 20170915.Earth System Grid
506 Federation. <https://doi.org/10.22033/ESGF/CMIP6.2463>

507 Roberts, C. D., R. Senan, F. Molteni, S. Boussetta, S. Keeley, 2017b: ECMWF ECMWF-IFS-
508 HR model output prepared for CMIP6 HighResMIP. Version 20170915.Earth System Grid
509 Federation. <https://doi.org/10.22033/ESGF/CMIP6.2461>

510 Roberts, M. J., and Coauthors, 2015: Tropical cyclones in the UPSCALE ensemble of high-
511 resolution global climate models. *Journal of Climate*, **28**, 574-596.

512 Roberts, M., 2017a: MOHC HadGEM3-GC31-LM model o 1008 utput prepared for CMIP6
513 HighResMIP. Version 20170906.Earth System Grid Federation.
514 <https://doi.org/10.22033/ESGF/CMIP6.1321>

515 Roberts, M., 2017b: MOHC HadGEM3-GC31-MM model output prepared for CMIP6
516 HighResMIP. Version 20180818.Earth System Grid Federation.
517 <https://doi.org/10.22033/ESGF/CMIP6.1902>

518 Roberts, M., 2017c: MOHC HadGEM3-GC31-HM model output prepared for CMIP6
519 HighResMIP. Version 20170831.Earth System Grid
520 Federation.<https://doi.org/10.22033/ESGF/CMIP6.446>

521 Roberts, M. J., and Coauthors, 2019a: Description of the resolution hierarchy of the global
522 coupled HadGEM3-GC313-GC3.1 model as used in CMIP6 HighResMIP experiments.
523 *Geosci. Model Dev.*, **12**, 4999-5028.

524 Roberts, M. J., 2019b: CMIP6 HighResMIP: Tropical storm tracks as calculated by the TRACK
525 algorithm. Centre for Environmental Data Analysis, 2019.
526 <http://catalogue.ceda.ac.uk/uuid/0b42715a7a804290afa9b7e31f5d7753>

527 Roberts, M. J., and Coauthors, 2020: Impact of model resolution on tropical cyclone simulation
528 using the HighResMIP-PRIMAVERA multi-model ensemble. *Journal of Climate*, **33**, 2557-
529 2583.

530 Scoccimarro, E., S. Gualdi, G. Villarini, G. A. Vecchi, M. Zhao, K. Walsh, and A. Navarra,
531 2014: Intense precipitation events associated with landfalling tropical cyclones in response to
532 a warmer climate and increased CO2. *Journal of climate*, **27**, 4642-4654.

533 Scoccimarro, E., A. Bellucci, D. Peano, 2017a: CMCC CMCC-CM2-HR4 model output
534 prepared for CMIP6 HighResMIP. Version YYYYMMDD[1].Earth System Grid Federation.
535 <https://doi.org/10.22033/ESGF/CMIP6.1359>

536 Scoccimarro, E., A. Bellucci, D. Peano, 2017b: CMCC CMCC-CM2-VHR4 model output
537 prepared for CMIP6 HighResMIP. Version YYYYMMDD[1].Earth System Grid Federation.
538 <https://doi.org/10.22033/ESGF/CMIP6.1367>

539 Scoccimarro, E., G. Villarini, S. Gualdi, A. Navarra, G. Vecchi, K. Walsh, and M. Zhao, 2017c:
540 Tropical cyclone rainfall changes in a warmer climate. *Hurricanes and Climate Change*,
541 Springer, 243-255.

542 Scoccimarro E., Gualdi S., Bellucci A. , Peano D., Cherchi A., Vecchi G.A. , Navarra A. 2020:
543 The typhoon-induced drying of the Maritime Continent. PNAS doi:
544 10.1073/pnas.1915364117.

545 Shepherd, J. M., A. Grundstein, and T. L. Mote, 2007: Quantifying the contribution of tropical
546 cyclones to extreme rainfall along the coastal southeastern United States. *Geophysical*
547 *Research Letters*, **34**.

548 Tang, X., W.-C. Lee, and M. Bell, 2014: A squall-line-like principal rainband in Typhoon
549 Hagupit (2008) observed by airborne Doppler radar. *Journal of the Atmospheric Sciences*,
550 **71**, 2733-2746.

551 Taylor, K.E., D. Williamson and F. Zwiers, 2000: The sea surface temperature and sea ice
552 concentration boundary conditions for AMIP II simulations. In PCMDI Report 60, Program
553 for Climate Model Diagnosis and Intercomparison, Lawrence Livermore National
554 Laboratory, 25 pp.

555 Touma, D., S. Stevenson, S. J. Camargo, D. E. Horton, and N. S. Diffenbaugh, 2019: Variations
556 in the intensity and spatial extent of tropical cyclone precipitation. *Geophysical Research*
557 *Letters*, **46**, 13992-14002.

558 Van Oldenborgh, G. J., and Coauthors, 2017: Attribution of extreme rainfall from Hurricane
559 Harvey, August 2017. *Environmental Research Letters*, **12**, 124009.

560 Vecchi, G. A., and Coauthors, 2019: Tropical cyclone sensitivities to CO2 doubling: roles of
561 atmospheric resolution, synoptic variability and background climate changes. *Climate*
562 *Dynamics*, **53**, 5999-6033.

563 Villarini, G., J. A. Smith, M. L. Baeck, T. Marchok, and G. A. Vecchi, 2011: Characterization of
564 rainfall distribution and flooding associated with U.S. landfalling tropical cyclones: Analyses
565 of Hurricanes Frances, Ivan, and Jeanne (2004). *Journal of Geophysical Research:*
566 *Atmospheres*, **116**.

567 Villarini, G., R. Goska, J.A. Smith, and G.A. Vecchi, North Atlantic tropical cyclones and U.S.
568 flooding, *Bulletin of the American Meteorological Society*, 95(9), 1381-1388, 2014a.

569 Villarini, G., and R. F. Denniston, 2016: Contribution of tropical cyclones to extreme rainfall in
570 Australia. *International Journal of Climatology*, **36**, 1019-1025.

571 Villarini, G., and Coauthors, 2014b: Sensitivity of tropical cyclone rainfall to idealized global-
572 scale forcings. *Journal of climate*, **27**, 4622-4641.

573 Voltaire, A., and Coauthors, 2019: Evaluation of CMIP6 DECK Experiments With CNRM-
574 CM6-1. *Journal of Advances in Modeling Earth Systems*, **11**, 2177-2213.

575 Vanniere, B., and Coauthors, The moisture budget of tropical cyclones: large scale environmental
576 constraints and sensitivity to model horizontal resolution, *Journal of Climate*, 33, 8457-8474.

577 Voltaire, A., 2018: CNRM-CERFACS CNRM-1092 CM6-1 model output prepared for CMIP6
578 HighResMIP. Earth System Grid Federation.
579 [http://cera1094www.dkrz.de/WDCC/meta/CMIP6/CMIP6.HighResMIP.CNRM-](http://cera1094www.dkrz.de/WDCC/meta/CMIP6/CMIP6.HighResMIP.CNRM-CERFACS.CNRM1095CM6-1)
580 [CERFACS.CNRM1095CM6-1](http://cera1094www.dkrz.de/WDCC/meta/CMIP6/CMIP6.HighResMIP.CNRM-CERFACS.CNRM1095CM6-1)

581 Voltaire, A., 2017: CNRM-CERFACS CNRM-CM6-1-HR model output prepared for CMIP6
582 HighResMIP. Earth System Grid Federation.
583 [http://cera1098www.dkrz.de/WDCC/meta/CMIP6/CMIP6.HighResMIP.CNRM-](http://cera1098www.dkrz.de/WDCC/meta/CMIP6/CMIP6.HighResMIP.CNRM-CERFACS.CNRM1099CM6-1-HR)
584 [CERFACS.CNRM1099CM6-1-HR](http://cera1098www.dkrz.de/WDCC/meta/CMIP6/CMIP6.HighResMIP.CNRM-CERFACS.CNRM1099CM6-1-HR)

585 von Storch, J.-S., and Coauthors, 2017: MPI-M MPI-ESM1.2-HR model output prepared for
586 CMIP6 HighResMIP. Earth System Grid Federation.

587 <http://cera1105www.dkrz.de/WDCC/meta/CMIP6/CMIP6.HighResMIP.MPI-M.MPI-ESM1->
588 2-HR

589 von Storch, J.-S., and Coauthors, 2019: MPI-M MPI-ESM1.2-XR model output prepared for
590 CMIP6 HighResMIP. Earth System Grid Federation.
591 <http://cera1108www.dkrz.de/WDCC/meta/CMIP6/CMIP6.HighResMIP.MPI-M.MPI-ESM1->
592 2-XR

593 Wang, S. S., L. Zhao, J.-H. Yoon, P. Klotzbach, and R. R. Gillies, 2018: Quantitative attribution
594 of climate effects on Hurricane Harvey’s extreme rainfall in Texas. *Environmental Research*
595 *Letters*, **13**, 054014.

596 Wang, Y., K.-H. Lee, Y. Lin, M. Levy, and R. Zhang, 2014: Distinct effects of anthropogenic
597 aerosols on tropical cyclones. *Nature Climate Change*, **4**, 368-373.

598 Wehner, M. F., and Coauthors, 2014: The effect of horizontal resolution on simulation quality in
599 the Community Atmospheric Model, CAM 5.1. *Journal of Advances in Modeling Earth*
600 *Systems*, **6**, 980-997.

601 Wright, D. B., T. R. Knutson, and J. A. Smith, 2015: Regional climate model projections of
602 rainfall from US landfalling tropical cyclones. *Climate dynamics*, **45**, 3365-3379.

603 Yu, Z., Y. Wang, H. Xu, N. Davidson, Y. Chen, Y. Chen, and H. Yu, 2017: On the relationship
604 between intensity and rainfall distribution in tropical cyclones making landfall over China.
605 *Journal of Applied Meteorology and Climatology*, **56**, 2883-2901.

606 Zhang, M., X. Chen, M. Kumar, M. Marani, and M. Goralczyk (2017). Hurricanes and tropical
607 storms: A necessary evil to ensure water supply? *Hydrological Processes*, **31**, 4414–4428.
608 <https://doi.org/10.1002/hyp.11371>

609 Zhang, W., and Coauthors, 2015: Improved Simulation of Tropical Cyclone Responses to ENSO
610 in the Western North Pacific in the High-Resolution GFDL HiFLOR Coupled Climate
611 Model. *Journal of Climate*, **29**, 1391-1415.

612 Zhang, W., G. Villarini, G. A. Vecchi, and J. A. Smith, 2018: Urbanization exacerbated the
613 rainfall and flooding caused by hurricane Harvey in Houston. *Nature*, **563**, 384-388.

614 Zhang, W., G. Villarini, G. A. Vecchi, and H. Murakami, 2019: Rainfall from tropical cyclones:
615 high-resolution simulations and seasonal forecasts. *Climate Dynamics*, **52**, 5269-5289.

616 Zhao, C., Y. Lin, F. Wu, Y. Wang, Z. Li, D. Rosenfeld, and Y. Wang, 2018: Enlarging rainfall
617 area of tropical cyclones by atmospheric aerosols. *Geophysical Research Letters*, **45**, 8604-
618 8611.

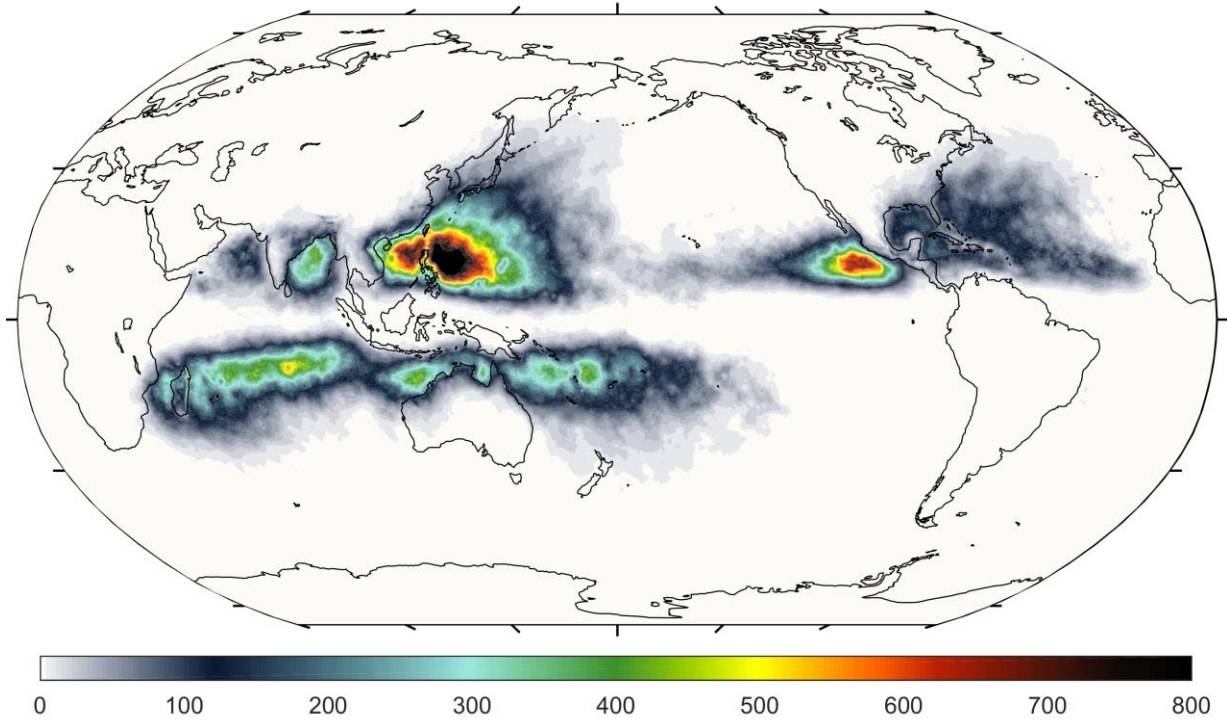
619 Zhao, M., I. M. Held, S.-J. Lin, and G. A. Vecchi, 2009: Simulations of global hurricane
620 climatology, interannual variability, and response to global warming using a 50-km
621 resolution GCM. *Journal of Climate*, **22**, 6653-6678.

622

623

624

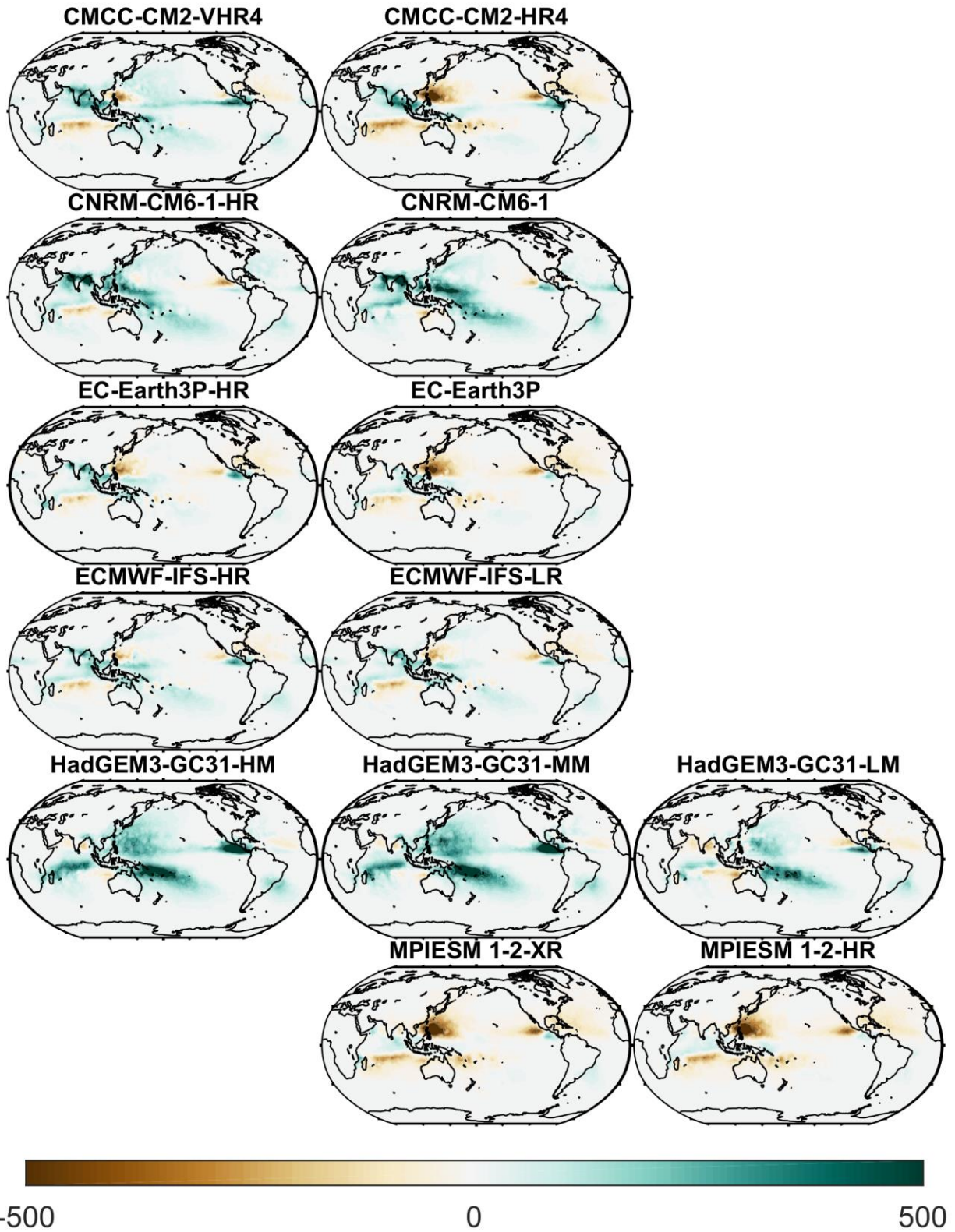
625



626

627 Figure 1 Annual average TC rainfall (unit: mm/year) in observations.

628

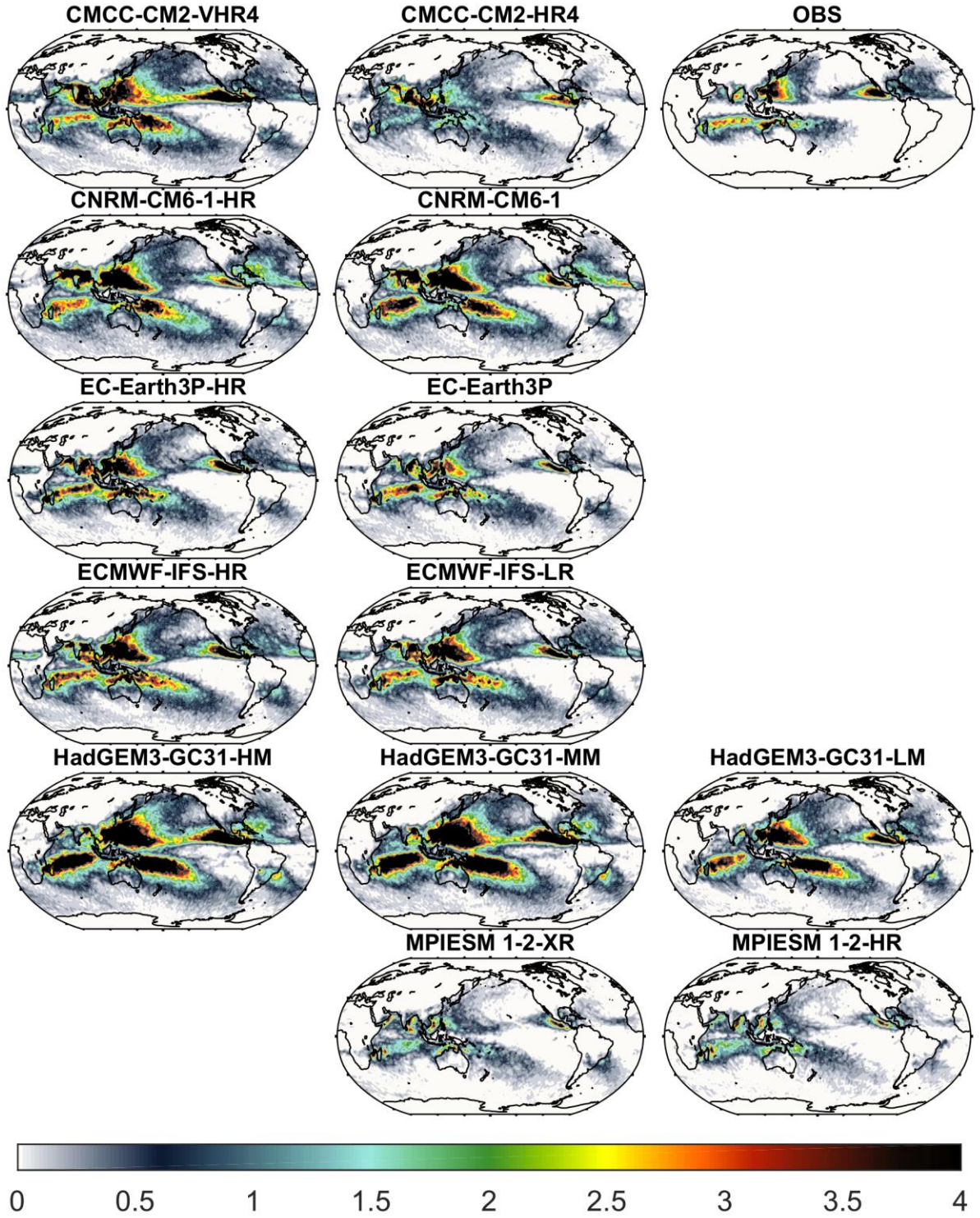


629

630

631

Figure 2. Differences in annual average TC rainfall (unit: mm/year) between observations and climate models archived in the PRIMAVERA Project (model minus observations).

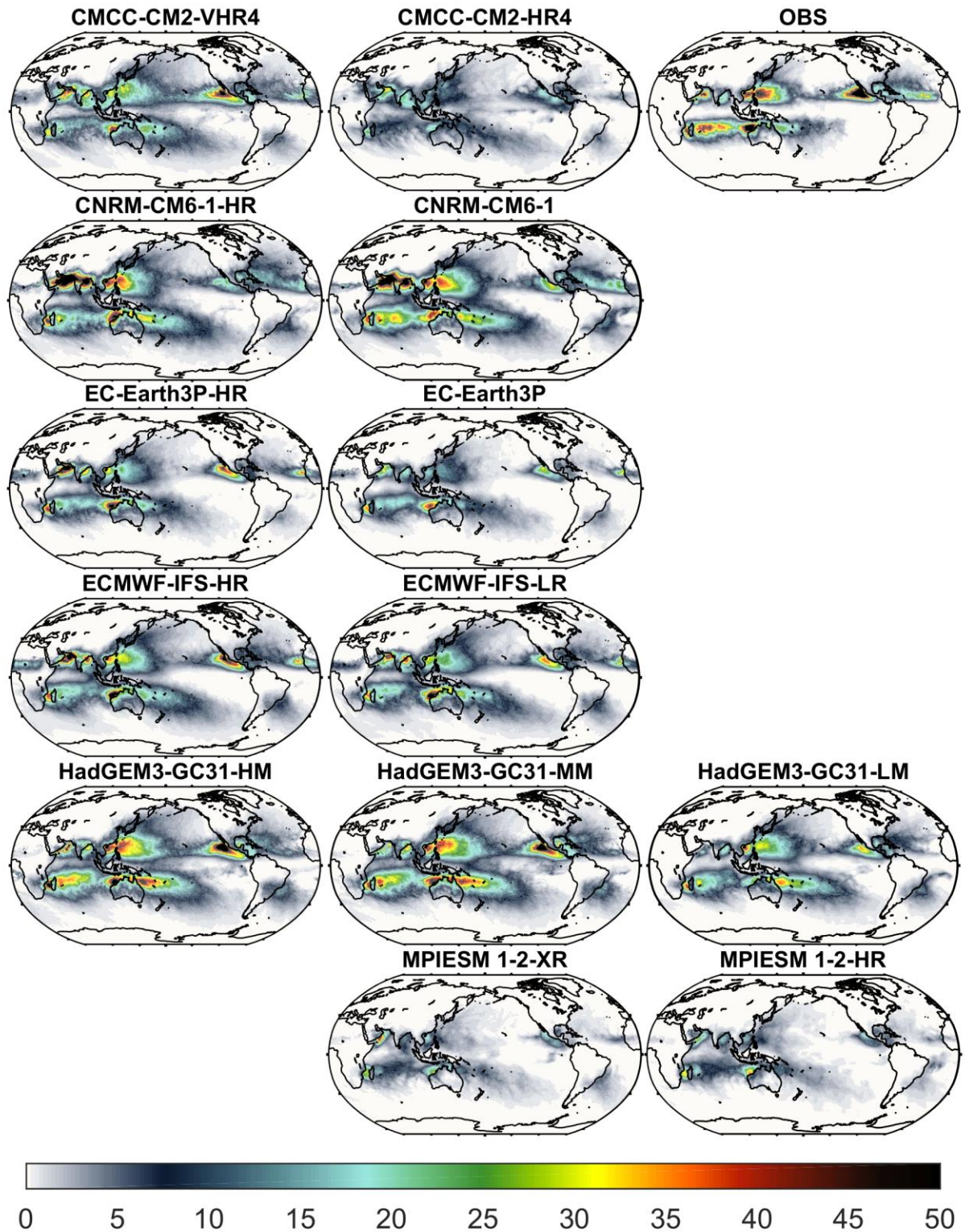


632

633 Figure 3. Annual average TC track density obtained by binning TC tracks into 2x2 spatial
 634 boxes in observations and climate models archived in the PRIMAVERA Project.

635

636

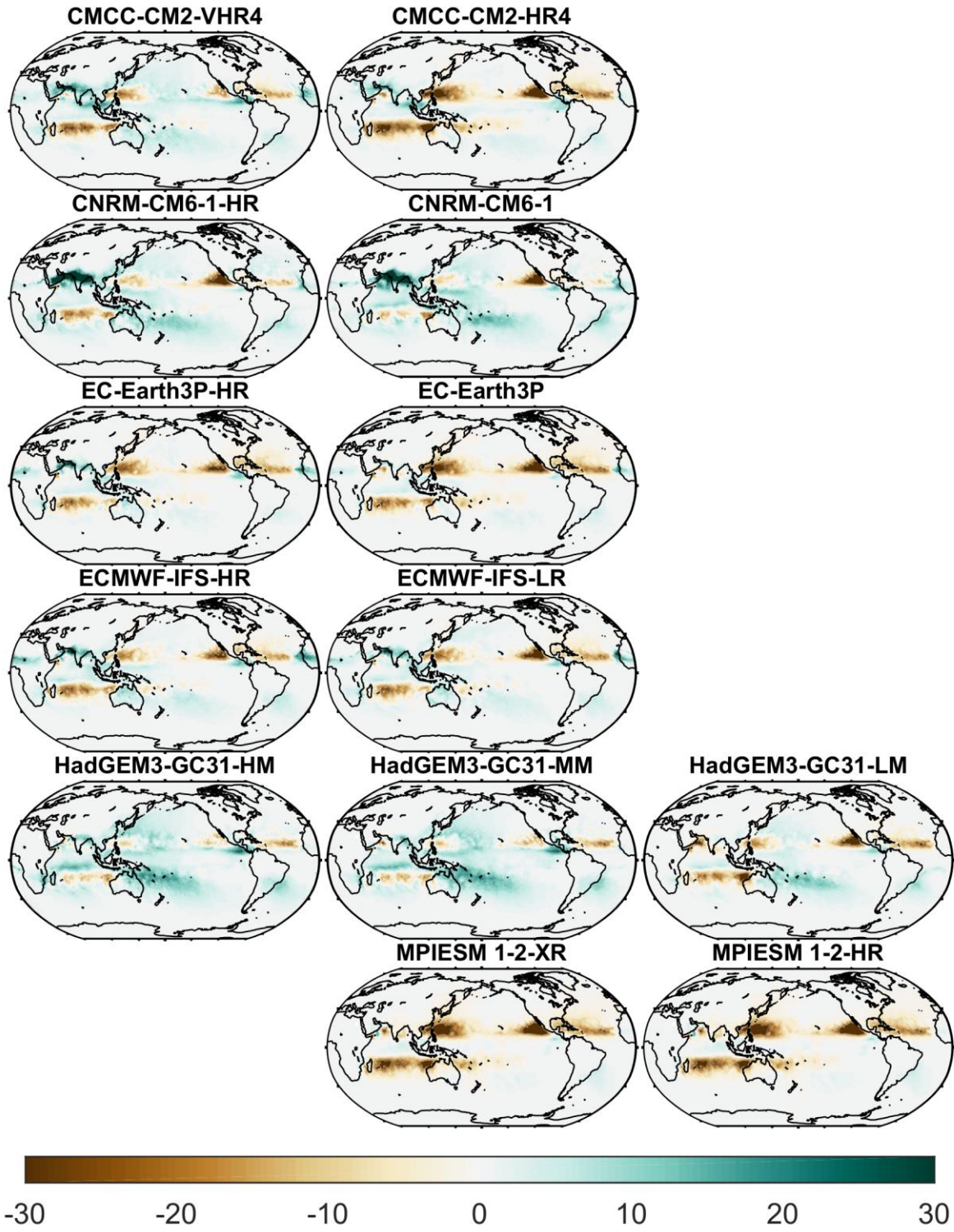


637

638

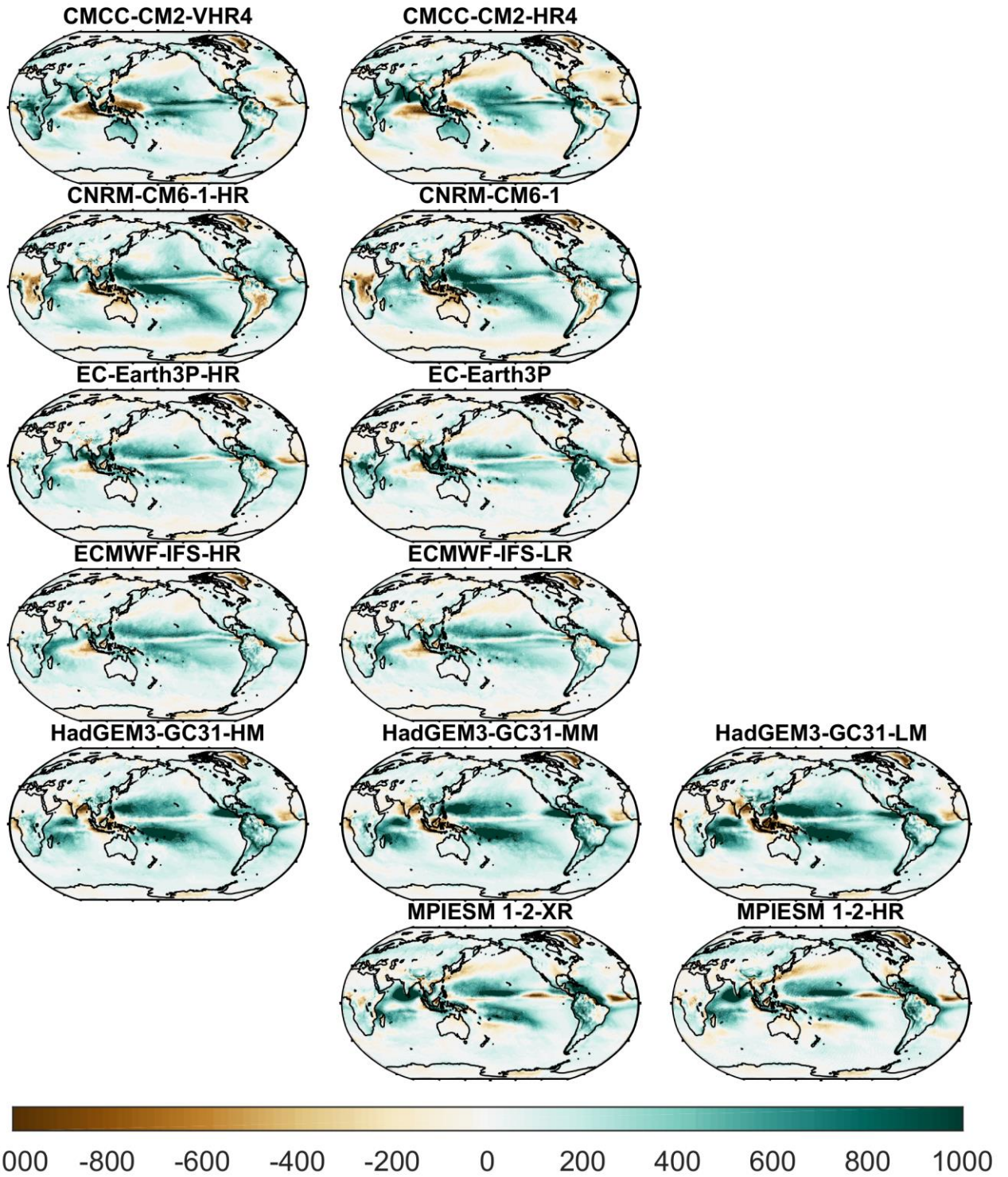
639

Figure 4. Percentage contribution of TC rainfall to total rainfall (unit: %) in observations and climate models archived in the PRIMAVERA Project.



640
641
642
643

Figure 5. Bias (model minus observations) in the percentage contribution of TC rainfall to total rainfall (unit: %) in the models.

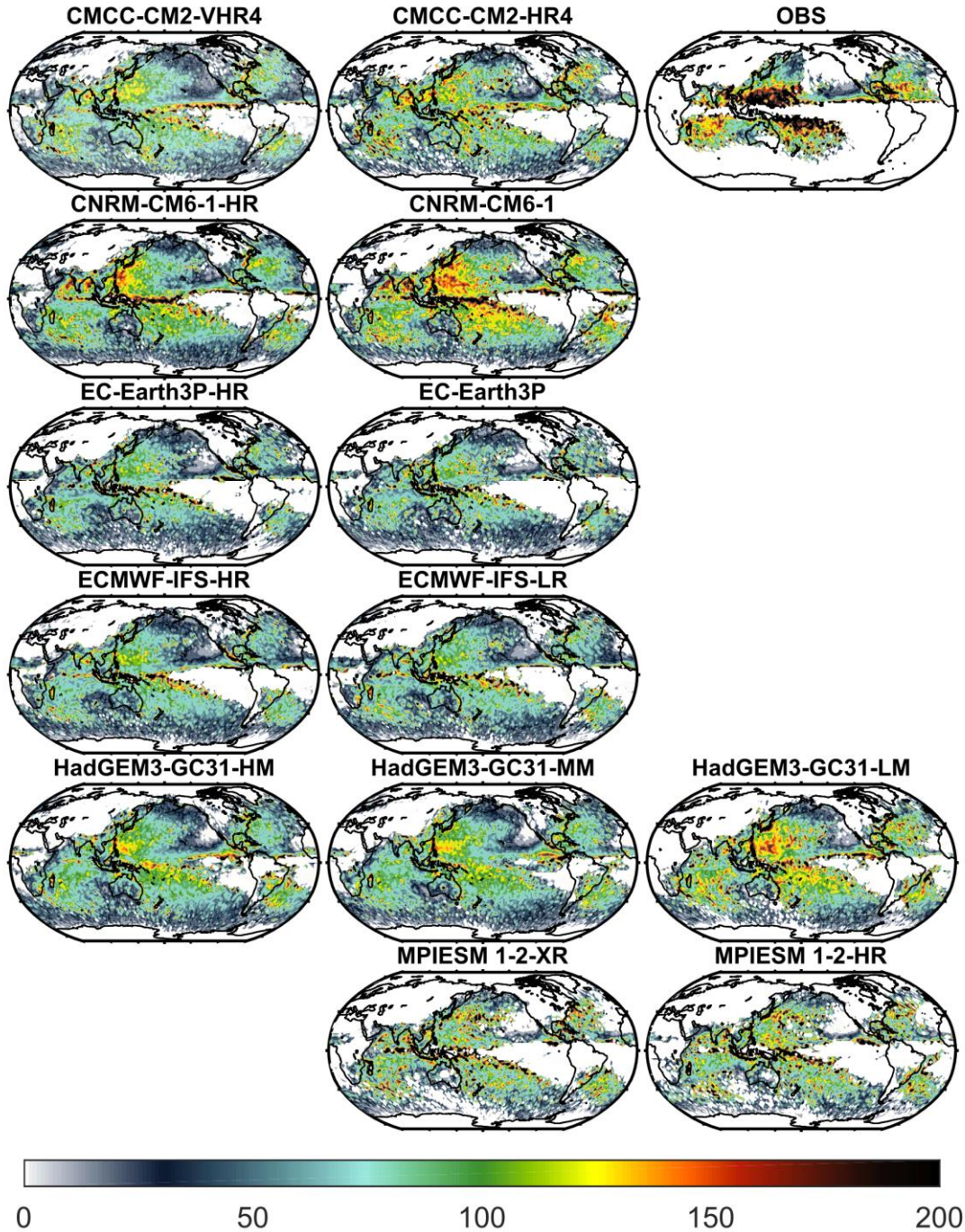


644

645 Figure 6. Bias (model minus observations) in total rainfall (unit: mm/year) in the models.

646

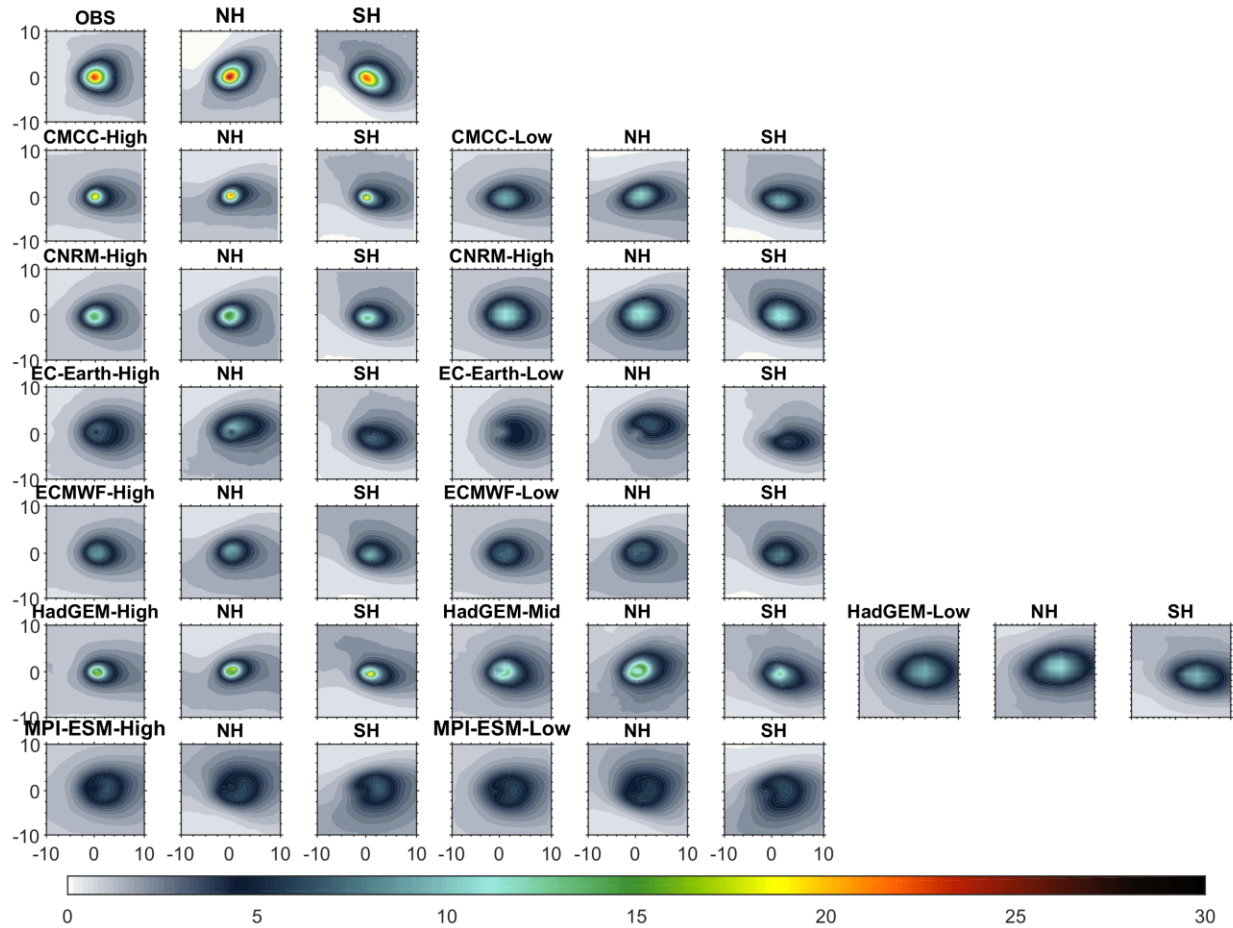
647



649

650 Figure 7. Average rainfall divided by TC track density (unit: mm) in observations and climate
 651 models archived in the PRIMAVERA Project. Average rainfall per TC track density represent
 652 the annual total TC rainfall divided by TC track density obtained by binning TC tracks into
 653 2×2 spatial boxes.

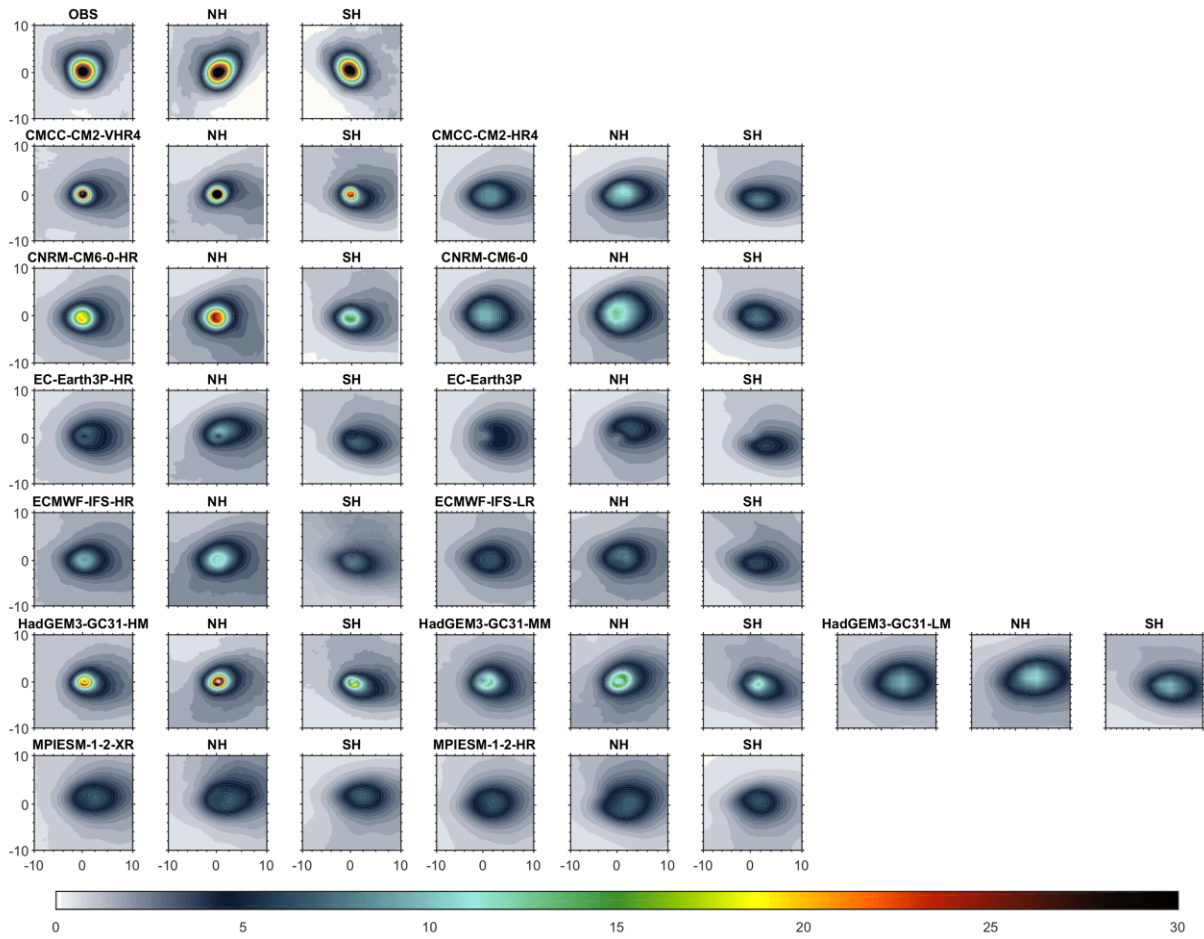
654



656

657 Figure 8. Composite 6-hour TC Rainfall (unit: mm) over the ocean & land in observations and
 658 climate models archived in the PRIMAVERA Project. The model resolution drops from left
 659 (columns 1-3) to right (columns 4-6 and 7-9). Every group of three columns represents the
 660 composite for all the storms, those in the northern hemisphere and those in the southern
 661 hemisphere.

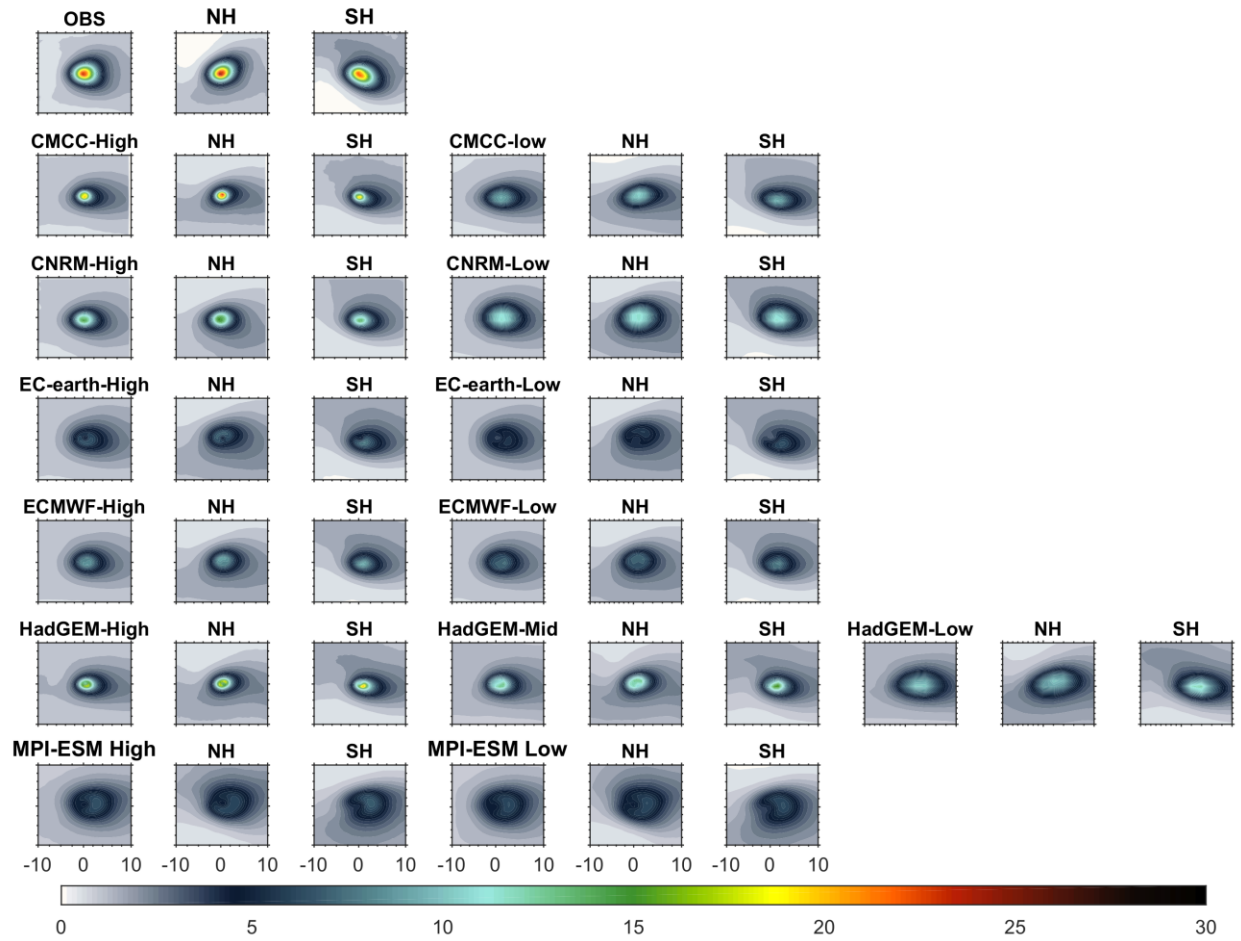
662



663

664 Figure 9. Composite 6-hour TC rainfall (unit: mm) across the 200 TCs with strongest intensity
 665 (sea level pressure) over the land and ocean in observations and climate models archived in the
 666 PRIMAVERA Project during 1980-2010. The model resolution drops from left (columns 1-3)
 667 to right (columns 4-6 and 7-9).

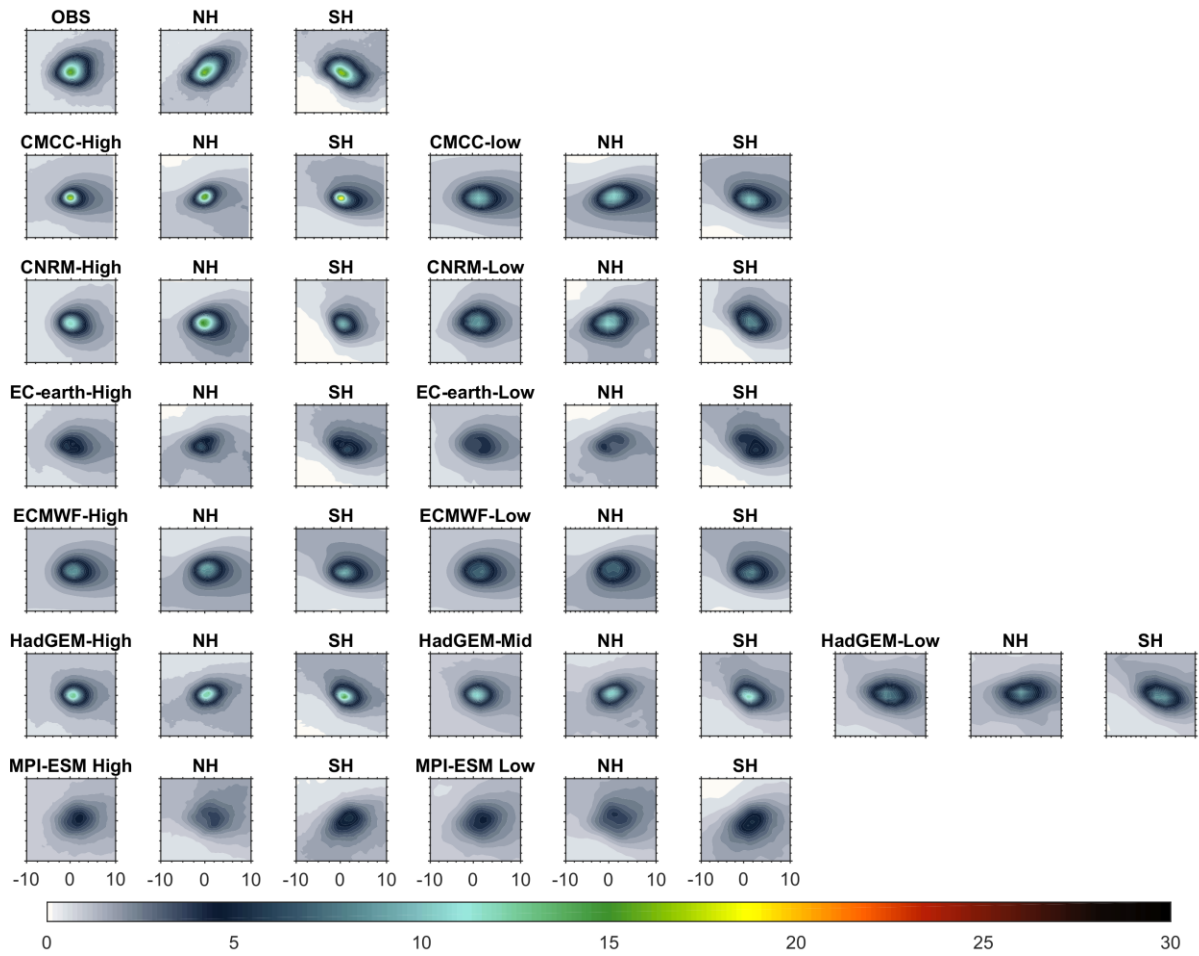
668



669

670

Figure 10. Same as Figure 8 but over ocean.



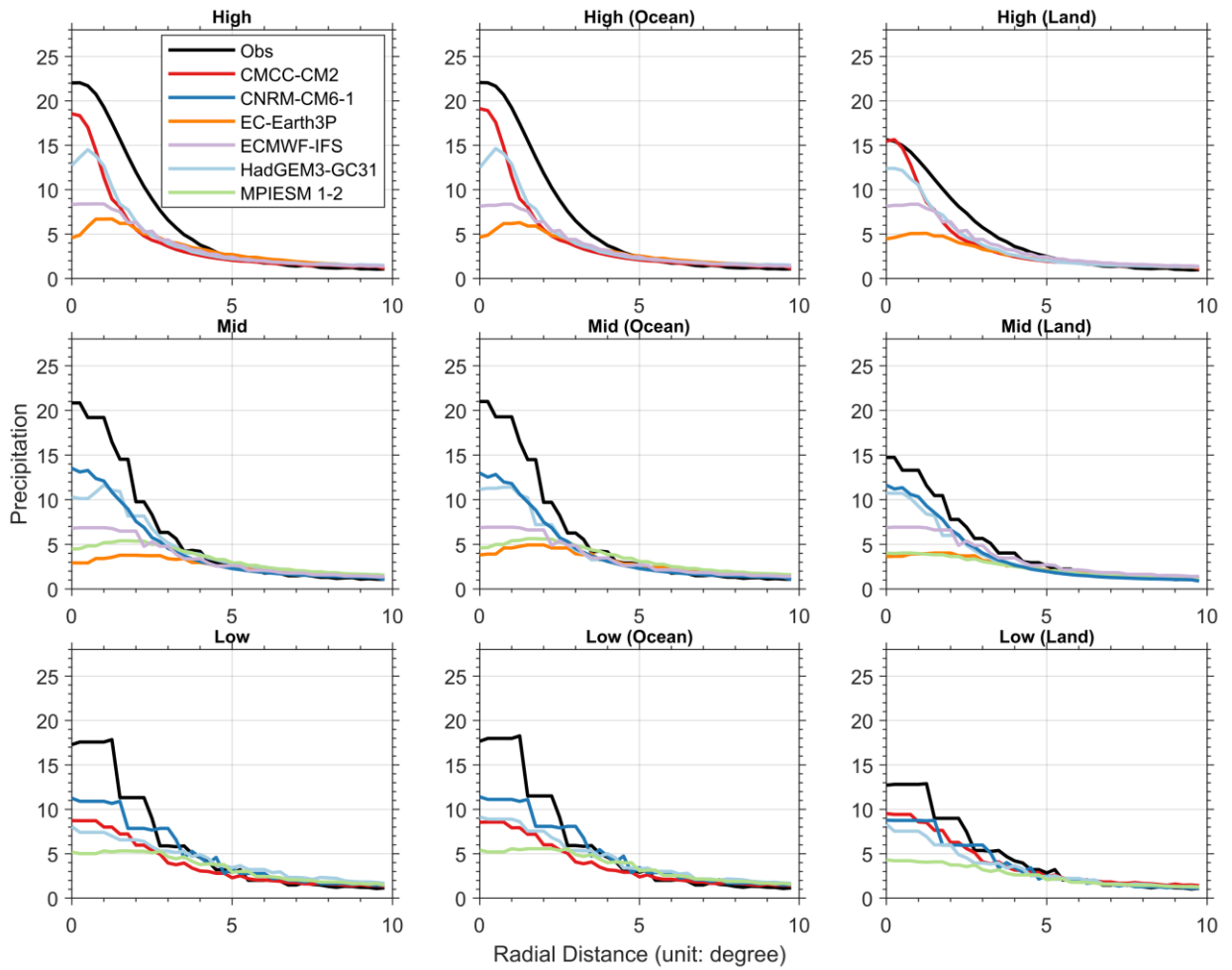
671

672 Figure 11. Same as Figure 8 but over land.

673

674

675



676

677 Figure 12. Radial profile of composite 6-hour TC rainfall (unit: mm) in observations and
678 models grouped into high-, mid-, and low-resolution climate models. The spatial resolution of
679 observed TC rainfall is re-gridded to each group (High, Mid and Low resolution) of the models.

680

681

682 Table 1. Spatial grids of the climate model outputs in high-, middle- and low-resolution groups
 683 used in this study. While ECMWF IFS data provided to HighResMIP are based on a reduced-
 684 resolution regular grid, the original ECMWF-IFS output uses the cubic octahedral reduced
 685 Gaussian grid, with resolutions of Tco399 (~25 km) and Tco199 (~50 km) for the HR and LR
 686 configurations, respectively.

Model	High	Middle/Medium	Low
CMCC-CM2	1152×768		288×192
CNRM-CM6-1		720×360	256×128
EC-Earth3P	1024×512	512×256	
ECMWF-IFS	720×361	360×181	
HadGEM3-GC313	1024×768	432×324	192×144
MPI-ESM1-2		768×384	384×192

687

688

689

690

691

692

693

694

695

696 Table 2 Definitions of basin boundaries

Basins	Boundary
Western North Pacific (WNP)	0-60°N, 100°E-180
Eastern North Pacific (ENP)	0-60°N, 180-100°W
North Atlantic (NA)	0-60°N, 100°W-0
North Indian Ocean (NI)	0-45°N, 45°E-100°E
South-West Indian Ocean (SI)	0-40°S, 0-90°E
South Pacific & Australia (SP)	0-40°S, 90°E-120°W
South Atlantic (SA)	0-60°S, 60°W-0

697

698

699

700

701

702 Table 3 Correlation between observed and simulated tropical cyclone rainfall across the globe
 703 and in different basins.

	Globe	WNP	ENP	NA	NI	SI	SP
CMCC-CM2-VHR4	0.77	0.87	0.77	0.68	0.83	0.80	0.76
CMCC-CM2-HR4	0.54	0.62	0.59	0.41	0.77	0.80	0.61
CNRM-CM6-1-HR	0.80	0.94	0.29	0.80	0.70	0.84	0.79
CNRM-CM6-1	0.81	0.89	0.41	0.82	0.74	0.88	0.72
EC-Earth3P-HR	0.85	0.89	0.37	0.77	0.89	0.86	0.90
EC-Earth3P	0.83	0.85	0.33	0.78	0.92	0.88	0.89
ECMWF-IFS-HR	0.87	0.92	0.71	0.79	0.87	0.84	0.85
ECMWF-IFS-LR	0.86	0.92	0.66	0.80	0.88	0.81	0.85
HadGEM3-GC31-HM	0.83	0.94	0.74	0.71	0.62	0.86	0.78
HadGEM3-GC31-MM	0.83	0.93	0.71	0.71	0.70	0.85	0.76
HadGEM3-GC31-LM	0.83	0.94	0.69	0.75	0.76	0.86	0.71
MPIESM 1-2-XR	0.67	0.68	0.26	0.64	0.81	0.73	0.81
MPIESM 1-2-HR	0.71	0.76	0.13	0.75	0.91	0.74	0.82

704

705 Table 4 Root mean square error (unit: mm) between observed and simulated tropical cyclone
 706 rainfall across the globe and in different basins.

	Globe	WNP	ENP	NA	NI	SI	SP
CMCC-CM2-VHR4	73.39	97.99	61.43	84.63	151.15	64.61	77.94
CMCC-CM2-HR4	79.44	152.37	14.90	80.66	140.61	83.06	74.72
CNRM-CM6-1-HR	95.27	136.22	27.57	46.58	280.06	61.12	67.15
CNRM-CM6-1	106.18	171.88	31.54	53.07	267.48	82.55	80.14
EC-Earth3P-HR	50.48	85.67	14.43	53.69	99.63	54.91	50.96
EC-Earth3P	54.26	125.33	13.08	51.90	40.53	51.50	42.83
ECMWF-IFS-HR	51.28	75.38	16.20	50.56	90.48	58.20	64.27
ECMWF-IFS-LR	49.17	75.97	15.91	44.59	93.09	62.63	61.00
HadGEM3-GC31-HM	129.29	159.11	59.40	161.02	75.63	151.65	143.76
HadGEM3-GC31-MM	130.32	173.13	56.98	151.07	68.51	145.72	147.59
HadGEM3-GC31-LM	76.46	96.64	25.58	62.46	45.38	70.04	96.37
MPIESM 1-2-XR	72.34	171.84	14.29	61.76	43.83	74.66	64.69
MPIESM 1-2-HR	69.57	167.61	14.15	57.32	31.24	72.98	61.12

707

708

709 Table 5 Correlation between observed and simulated tropical cyclone rainfall proportion across
 710 the globe and in different basins.

	Globe	WNP	ENP	NA	NI	SI	SP
CMCC-CM2-VHR4	0.80	0.86	0.88	0.85	0.71	0.79	0.87
CMCC-CM2-HR4	0.65	0.72	0.71	0.64	0.67	0.79	0.86
CNRM-CM6-1-HR	0.71	0.92	0.55	0.75	0.64	0.85	0.86
CNRM-CM6-1	0.75	0.92	0.53	0.73	0.72	0.93	0.88
EC-Earth3P-HR	0.82	0.91	0.57	0.78	0.80	0.88	0.95
EC-Earth3P	0.81	0.90	0.53	0.72	0.87	0.89	0.95
ECMWF-IFS-HR	0.80	0.93	0.83	0.74	0.78	0.85	0.89
ECMWF-IFS-LR	0.79	0.92	0.79	0.70	0.80	0.82	0.91
HadGEM3-GC31-HM	0.86	0.93	0.78	0.87	0.84	0.88	0.83
HadGEM3-GC31-MM	0.85	0.92	0.71	0.86	0.80	0.88	0.82
HadGEM3-GC31-LM	0.79	0.94	0.67	0.81	0.64	0.90	0.69
MPIESM 1-2-XR	0.69	0.70	0.08	0.64	0.77	0.77	0.89
MPIESM 1-2-HR	0.73	0.77	-0.05	0.67	0.83	0.77	0.93

711

712

713 Table 6 Root mean square error (unit: %) between observed and simulated tropical cyclone
 714 rainfall proportion across the globe and in different basins.

	Globe	WNP	ENP	NA	NI	SI	SP
CMCC-CM2-VHR4	5.10	5.90	3.41	5.32	9.66	7.93	6.43
CMCC-CM2-HR4	6.58	9.13	2.11	8.61	6.89	9.81	9.88
CNRM-CM6-1-HR	6.57	4.80	2.42	6.98	18.22	6.28	6.69
CNRM-CM6-1	6.26	4.85	2.50	6.97	16.71	4.66	6.14
EC-Earth3P-HR	4.80	6.20	2.41	6.70	7.95	6.47	4.18
EC-Earth3P	5.44	8.59	2.66	8.08	3.73	7.07	5.34
ECMWF-IFS-HR	4.99	4.70	1.77	6.78	8.36	7.26	5.79
ECMWF-IFS-LR	5.03	5.51	1.92	7.49	7.24	7.09	5.03
HadGEM3-GC31-HM	5.14	5.92	3.29	4.92	5.28	6.48	7.99
HadGEM3-GC31-MM	5.14	5.75	3.14	5.14	5.21	5.96	8.26
HadGEM3-GC31-LM	5.10	4.23	2.09	6.82	6.07	5.86	8.78
MPIESM 1-2-XR	6.87	10.79	2.86	9.43	4.82	9.46	9.41
MPIESM 1-2-HR	6.68	10.66	2.90	9.42	4.37	9.23	8.10

715

716